ABSTRACT

Test of a Method for Recognizing Unmapped Seismogenic Faults

Brian G. Bayliss, M.S.

Thesis Chairperson: Vincent S. Cronin, Ph.D.

Using the seismo-lineament analysis method developed by Cronin (Gammill and others, 2004), I have attempted to locate Holocene faults in the Point Dume 7.5 minute quadrangle of the central Santa Monica Mountains, southern California. I projected the nodal planes from each of eight focal-mechanism solutions for earthquakes with reported epicenters within the Pt. Dume quadrangle to define their intersection with a digital elevation model (DEM) of the ground surface. The intersection of a nodal plane with the ground surface is termed a *seismo-lineament*. Mapping seismo-lineaments onto a DEM yielded specific fault-location hypotheses that can be tested in the field. Accessible outcrops and road cuts were examined along each seismo-lineament to look for evidence of faulting on planes that are approximately parallel to the nodal planes. Several previously unidentified potentially seismogenic faults have been identified in this study, indicating that the seismo-lineament method is useful.

Test of a Method for Recognizing Unmapped Seismogenic Faults

by

Brian G. Bayliss, B.S.

A Thesis

Approved by the Department of Geology

_____

Steven G. Driese, Ph.D., Chairperson

Submitted to the Graduate Faculty of
Baylor University in Partial Fulfillment of the
Requirements for the Degree
of
Master of Science

Approved by the Thesis Committee

_____

Vincent S. Cronin, Ph.D., Chairperson

_____

Tom T. Goforth, Ph.D.

_____

Joseph D. White, Ph.D.

Accepted by the Graduate School
May 2007

_____

J. Larry Lyon, Ph.D., Dean

TABLE OF CONTENTS

LIST OF FIGURES

ACKNOWLEDGMENTS

This study was sponsored by grants in aid of research from the Gulf Coast Association of Geological Societies and the Baylor University Department of Geology.

I want to thank Lisa M. Zygo for her assistance and GIS expertise. I want to thank Dr. Vincent S. Cronin for providing me with the opportunity to work on an exciting project as well as a fantastic study area. His expertise and guidance through this process were invaluable.

CHAPTER ONE

Introduction

Identifying active or potentially active faults is a challenging task, particularly in areas that have high relief, dense vegetation, restricted access, urban cover, or other conditions that make it difficult or expensive to conduct field work. Despite these challenges, it is necessary to identify active or potentially active faults to accurately assess the likelihood of future earthquakes that may affect a given area.

The work described in this thesis is part of an ongoing project involving a team of researchers under the direction of Vince Cronin at Baylor University. The team is developing an array of methods that are useful in defining specific areas that may contain the surface trace of an active fault. These methods generate hypotheses about potentially seismogenic faulting that can be tested through geologic fieldwork. This toolkit includes traditional methods of aerial photo analysis, analysis of digital data from satellites and aircraft to detect vegetation anomalies, analysis of surface geomorphology using digital elevation models (Cronin and others, 2003), and a method developed by Cronin involving projection of fault-plane solutions derived from published earthquake focal-mechanism solutions (Gammill and others, 2004).

Geologists have long been able to locate faults by noting characteristic geomorphic features like linear valleys, scarps transverse to drainages, truncated spurs, sags and pop-ups (*e.g.,* Lobeck, 1939; Worchester, 1948). The expression of faults at the ground surface has also made it possible to locate faults through methods of aerial photo interpretation

(*e.g.,* Hobbs, 1904; Ray, 1960; Miller, 1961) and analysis of satellite imagery (*e.g.,* Lillesand and Kiefer, 1987; Cronin and others, 1993). Development of technology to create an image of a surface derived from a digital elevation model (DEM) and illuminate that image from different directions has facilitated the identification of geomorphic lineaments that may be related to faults (*e.g.,* Haugerud and others, 2003; Cronin and others, 2003). In general, remote-sensing methods for the recognition of faults yield hypotheses for the possible location of faults, and these hypotheses need to be evaluated through geological field work. Faults found in this manner may be inactive or fossil faults, or they may still be subject to seismogenic displacement.

Geoscientists interested in identifying and characterizing seismogenic faults (*i.e.,* faults that generate earthquakes) generally utilize the tools of paleoseismology to conduct their studies (*e.g.,* McCalpin, 1996). These include aerial photo interpretation, surface geological mapping, and trenching across suspected fault traces in areas where there is a Holocene unit that may have been displaced by motion along the fault. Trench studies are expensive, require sufficient undeveloped space across the suspected fault trace to construct the trench with heavy equipment, often require special permits, and place the geoscientists who describe the trench in physical danger. If the units exposed at the surface along the fault trace do not contain Holocene material, trenching will not be able to demonstrate Holocene offset.

An approach to solving the problem of identifying seismogenic faults that do not cut Holocene material at the ground surface has been developed by Vince Cronin, who developed a method to project a fault-plane solution from an earthquake focus upward to define its intersection with a digital model of the ground surface. Cronin calls the

intersection of the fault-plane solution and the ground surface a *seismo-lineament*. This method has the promise of relating faults observed at the surface with recorded earthquakes for which focal-mechanism solutions have been derived.

The purpose of this thesis research is to test the idea of using seismo-lineaments to find potentially seismogenic faults – faults within the seismo-lineament that have approximately the same orientation and slip characteristics as the fault-plane solution that defined the corresponding seismo-lineament.

The field area used for this test is in the Point Dume 7.5 minute quadrangle in the central Santa Monica Mountains of southern California, which includes part of the surface trace of the Malibu Coast Fault Zone (MCFZ; fig. 1). The MCFZ is one of several fault systems that define the southern edge of the Transverse Ranges Province (Cronin and Sverdrup, 1998).

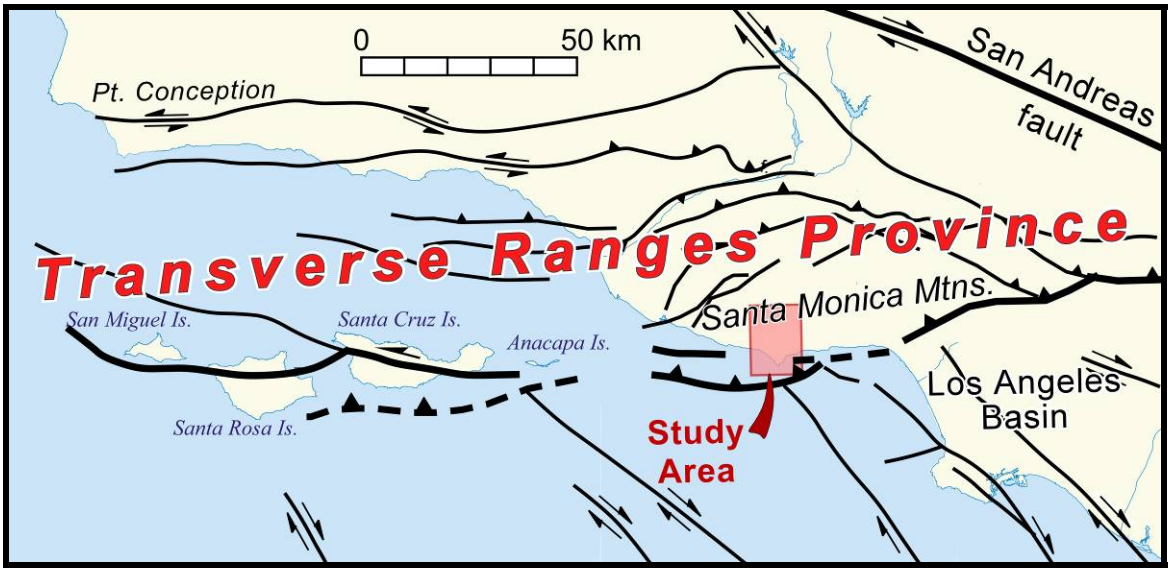

FIGURE 1. The location of the Point Dume Quadrangle within the structural context of southern California.

To the south of the MCFZ is the California Continental Borderland Province (Wright, 1991). Other major faults in this boundary-fault system, such as the Hollywood fault and the Raymond fault, are legally defined as active faults because of demonstrated offset of Holocene strata in trenches, whereas most elements of the MCFZ are not (as yet) designated as active faults (Cronin and Sverdrup, 1998; Hart and Bryant, 1999).

As defined by Cronin and Sverdrup (1998), "the Malibu Coast fault of the MCFZ is an anastamosing zone of fault strands within a few kilometers of the Malibu coastline," trending parallel to the coastline (fig. 2). Strands of the Malibu Coast fault generally dip toward the north at 30 to 70 degrees, and contain evidence of reverse oblique slip, typically with a left-lateral strike-slip component (Cronin and Sverdrup, 1998).

Current models suggest that a few small strands of the MCFZ and some offshore faults are the only potentially active faults in the area (fig. 3; Treiman, 1994). We are

FIGURE 2. Elements of the Malibu Coast Fault Zone along the southern edge of the central Santa Monica Mountains. The only strands of this fault zone that are considered "active" by the criteria of the Alquist-Priolo Act are the Solstice strand (S) and the Winter Mesa strand (WM), whose study-zone boundaries are outlined in red. The Potrero Fault (P) displays 47 meters of vertical displacement during the last 124,000 years (Hill, 1979; LaJoie and others, 1979).

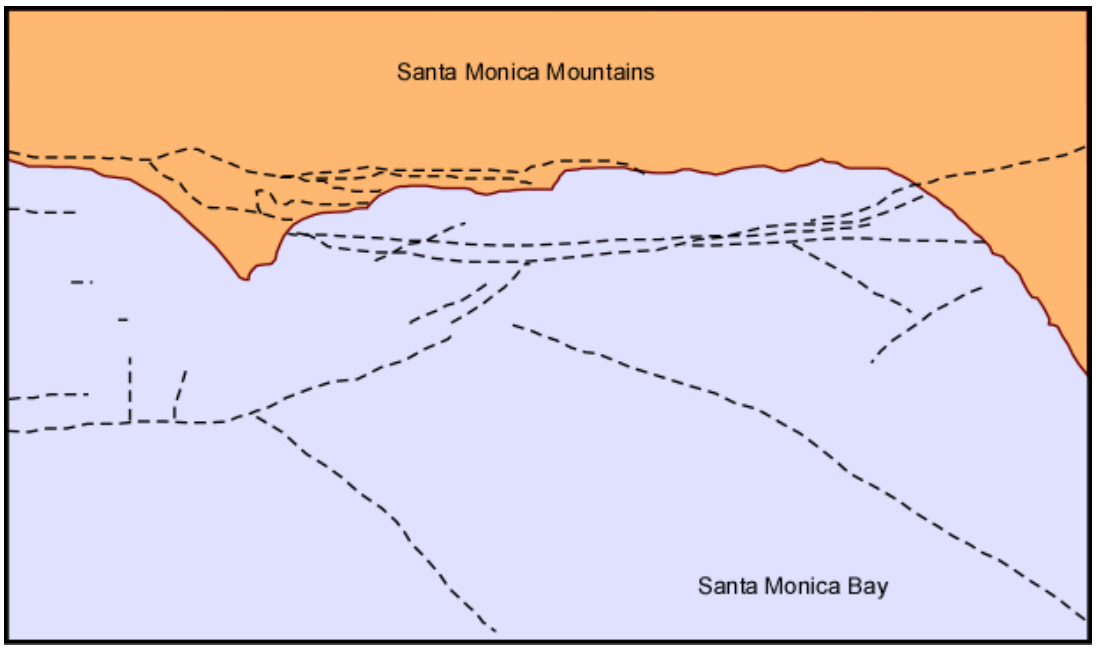

FIGURE 3. Map of faults along the southern edge of the Santa Monica Mountains and northern Santa Monica Bay thought by Treiman (1994) to be worthy of analysis for possible Holocene activity. The faults are confined to a narrow strip along the coast and the offshore area that is not subject to fault-hazard zonation under the Alquist-Priolo Act. No faults in the core of the Santa Monica Mountains were thought worthy of analysis for possible Holocene activity.

investigating the possibility that other faults in the Santa Monica Mountains may have been seismogenic during the Holocene.

CHAPTER TWO

Background

The study area is located in the western Transverse Ranges Province of southern California. Specifically, work was conducted in the Point Dume 7.5 minute Quadrangle within the Santa Monica Mountains, thirty miles west of downtown Los Angeles (fig. 2).

Southern California is one of the most geologically studied areas on Earth. The Greater Los Angeles area hosts a large population, many economic resources, complex geology and many geologic hazards. It is home to several major research universities with significant geoscience departments, including the California Institute of Technology (Caltech), the University of Southern California, several branches of the California State University System (*e.g.,* Los Angeles, Northridge, Fullerton, San Diego), several branches of the University of California System (Santa Barbara, Los Angeles, Riverside, San Diego) and a major marine laboratory (Scripps Institution). A consortium of these and other universities and the U.S. Geological Survey comprise the Southern California Earthquake Center (SCEC).

The tectonic regime of southern California is dominated by the complex interaction of slivers of continental crust that are in motion within the boundary zone between the North American and Pacific plates. The relative motion of the Pacific plate relative to the North American plate is currently ~47 mm/yr toward ~321° azimuth, determined at Point Dume (Cronin and Sverdrup, 1998). The present-day stresses may be characterized by transpressional crustal deformation inferred to be related to the restraining bend of the

San Andreas fault across the Transverse Ranges (Tsutsumi and others, 2001). Historical records of seismicity, geomorphic evidence and geodetic measurements indicate that compression and strike-slip motion both contribute to the tectonic deformation and the seismic hazard of the western Transverse Ranges (Ziony and Yerkes, 1985; Hauksson and Saldivar, 1989; Hauksson, 1987; Wesnousky, 1986; Dolan and others, 1995; Larsen and others, 1993; Larson, 1993; Molnar and Gibson, 1994; Pinter and others, 1998).

Paleomagnetic data suggests that the Transverse Ranges are rotating in a clockwise direction ~6 degrees per million years, and have done so for the past ~16-18 million years (Figure 4; Lajoie and others, 1979; Kamerling and Luyendyk, 1979; Luyendyk and others, 1985; Luyendyk, 1991; Hornafius and others, 1986). Legg and others (2004) have suggested that the cause of this rotation is traction along the base of the Transverse Ranges imparted by the underthrusting of parts of the California Continental Borderland, which is an adaptation of the microplate capture model as proposed by Nicholson and others, (1994). The Los Angeles Area Seismic Experiment II (LARSE II) showed the continental borderland seems to be underthrusting the Santa Monica Mountains (Fuis and others, 2003).

The Transverse Ranges are characterized by rates of uplift and convergence of ~4-10 mm per year (Lajoie and others, 1979; Kamerling and Luyendyk, 1979; Luyendyk and others, 1985; Luyendyk, 1991). The uplift of the Santa Monica Mountains has been attributed to the reverse component of slip on the Santa Monica, Dume, and Malibu Coast faults, combined with slip on a buried thrust surface (Pinter and others, 1998). However,

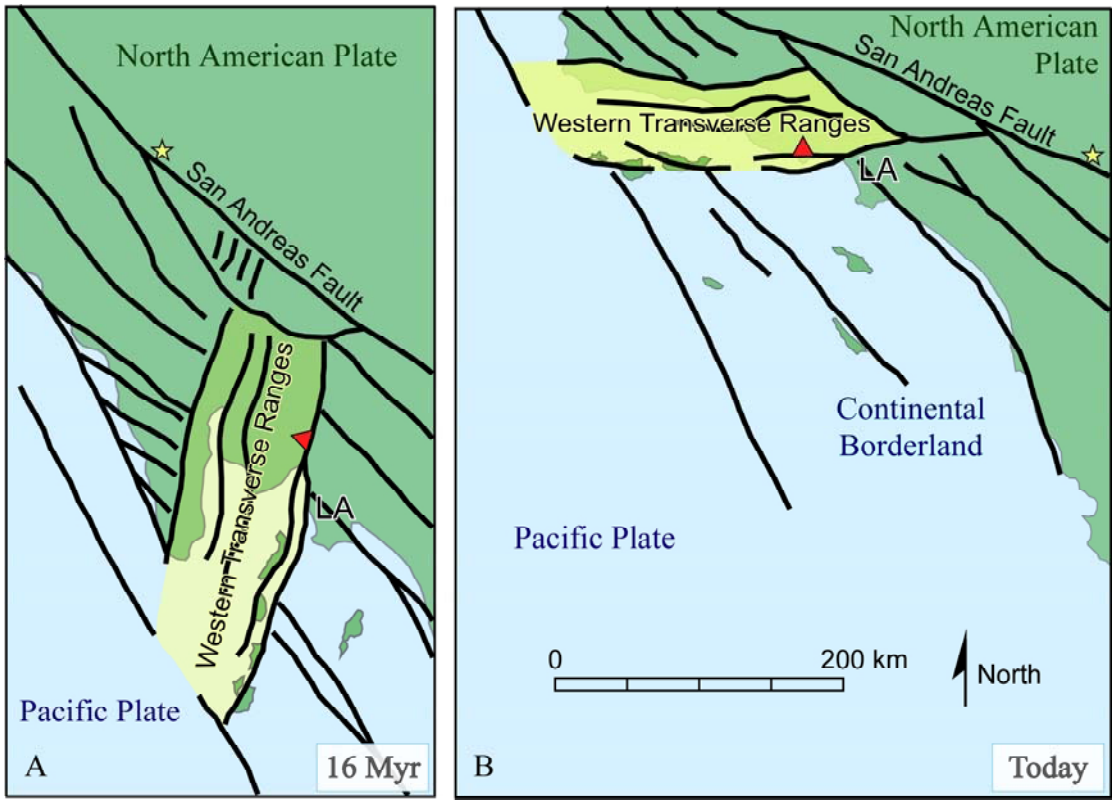

FIGURE 4. Rotation of western Transverse Ranges as supported by analysis of paleomagnetic vectors. The red triangle marks the position of Point Dume, and the star is the fixed frame of reference on the North American plate for both illustrations. (A) Configuration of crustal blocks between the Pacific and North American plates in southern California circa 16 Myr. (B) Present-day configuration of southern California showing major block-bounding faults. After Hornafius and others, 1986.

others attribute the uplift of the Santa Monica Mountains to a blind thrust called the Santa Monica thrust, which is similar to the Channel Islands thrust fault (*e.g.*, Davis and others, 1989; Dolan and others, 2000).

The rocks exposed in the central and western Santa Monica Mountains include Late Cretaceous to Pleistocene sedimentary rocks, which are primarily marine with a lesser constituent of terrestrial strata, and Miocene volcanic rocks (Blake, 1991; Fisher and

others, 2005; Wright, 1991). In the eastern Santa Monica Mountains, Cretaceous granite and meta-sedimentary rocks are exposed.

For the purpose of this study, a fault is defined as a surface or zone along which there is shear displacement (Cronin and Sverdrup, 1998). A fault is legally considered to be "active" by the State of California if Holocene displacement has been demonstrated by means of a trench study (Hart and Bryant, 1999; see discussion by Cronin and Sverdrup, 1998). The faults identified as a result of this study do not appear to cut Holocene deposits because they traverse highland areas that are prone to high rates of erosion rather than deposition. Consequently, there is little or no Holocene cover available to be displaced by faulting, apart from transient colluvium. This illustrates the inherent limitation of using only trench studies or observed surface rupture to define a fault as active.

The Malibu Coast Fault Zone is a set of east-west trending faults located within ~3 km of the Malibu coastline (onshore and offshore) that collectively mark the southern boundary of the Transverse Ranges in the central and western Santa Monica Mountains (Cronin and Sverdrup, 1998; Hornafius and others, 1986). One of the principal strands of the Malibu Coast Fault Zone is the Malibu Coast fault, whose trace is close to the pronounced slope break along the southern base of the Santa Monica Mountains. A trench study performed by Drumm (1992) determined that a central splay of the Malibu Coast fault has been active during the Holocene. Other studies suggest that the main trace of the fault has ***not*** been active during the Holocene, and is therefore considered inactive (Treiman, 1994). If strands or splays of the fault are considered active, it seems inconsistent that the whole system is not considered active.

The surface traces of the northwest-trending strike-slip faults of southern California terminate along (or are overthrust by) the north-dipping thrust faults at the southern edge of the Transverse Ranges. These sub-parallel right-lateral strike-slip faults include the Santa Rosa-Cortes Ridge fault, San Clemente Island fault, San Pedro Basin fault and Rose Canyon fault of the California Continental Borderland Province offshore, and the Newport-Inglewood, Whittier-Elsinore, and San Jacinto faults of the northern Peninsular Ranges Province onshore.

In addition to a component of reverse slip that is evident in the elevation difference between the high-ground north of the Malibu Coast Fault Zone and the low-ground to the south, there has been significant left-lateral strike slip along this trend. Lateral displacement along the Santa Monica/Malibu Coast fault has been estimated to be as much as 60-90 km since the Miocene (Cronin and Sverdrup, 1998).

Most of the damaging earthquakes in the Transverse Ranges have originated from structurally subtle and relatively short fault segments (*e.g.,* Hauksson, 1990; Seeber and Sorlien, 2000). Sorlien and others (2003) show that the Dume and Malibu Coast faults converge downward and can be projected into the aftershock zone of the 1973 Point Mugu earthquake. They have proposed that the 1973 Point Mugu quake (M 5.3) occurred along these faults.

The upper limit on the magnitude of possible earthquakes in the area may be greater than any of the historic earthquakes (Seeber and Sorlien, 2000). Dolan and others (1995) estimated that the Malibu Coast fault and the Santa Monica fault (another member of the regional fault system) could each cause earthquakes as large as M 7.0. However, only short segments of the Malibu Coast Fault Zone are officially recognized as active faults.

The M 6.7 Northridge earthquake of January 17, 1994, was caused by the rupture of a south dipping blind reverse fault that had not been previously recognized as a major seismic source (Davis and Namson, 1994; Yeats and Huftile, 1995). Any unknown seismogenic fault presents a dangerous problem for the populations that reside near it. Identifying potentially seismogenic faults has become important in evaluating the seismic hazards of the Los Angeles metropolitan area (Tsutsumi and others, 2001).

There are many mapped faults within the Santa Monica Mountains (fig 5). Field studies in the area indicate that there are also many unmapped faults, many of which have modest displacement and are assumed to be inactive. The catalog of historic earthquakes maintained by the National Geophysical Data Center, and other sources, demonstrate that there have been more than one thousand events reported in the area of the central and western Santa Monica Mountains and northern Santa Monica Bay (*e.g.,* Cronin and Sverdrup, 1998).

The occurrence of earthquakes is a good indicator that there are active faults in an area. Figure 6 shows that earthquake activity is not limited to the coastline and Santa Monica Bay but is present throughout the Santa Monica Mountains. This study will contribute to the current mapping of faults. Continued mapping will allow for better seismic risk assessment and more adequate building codes within the area.

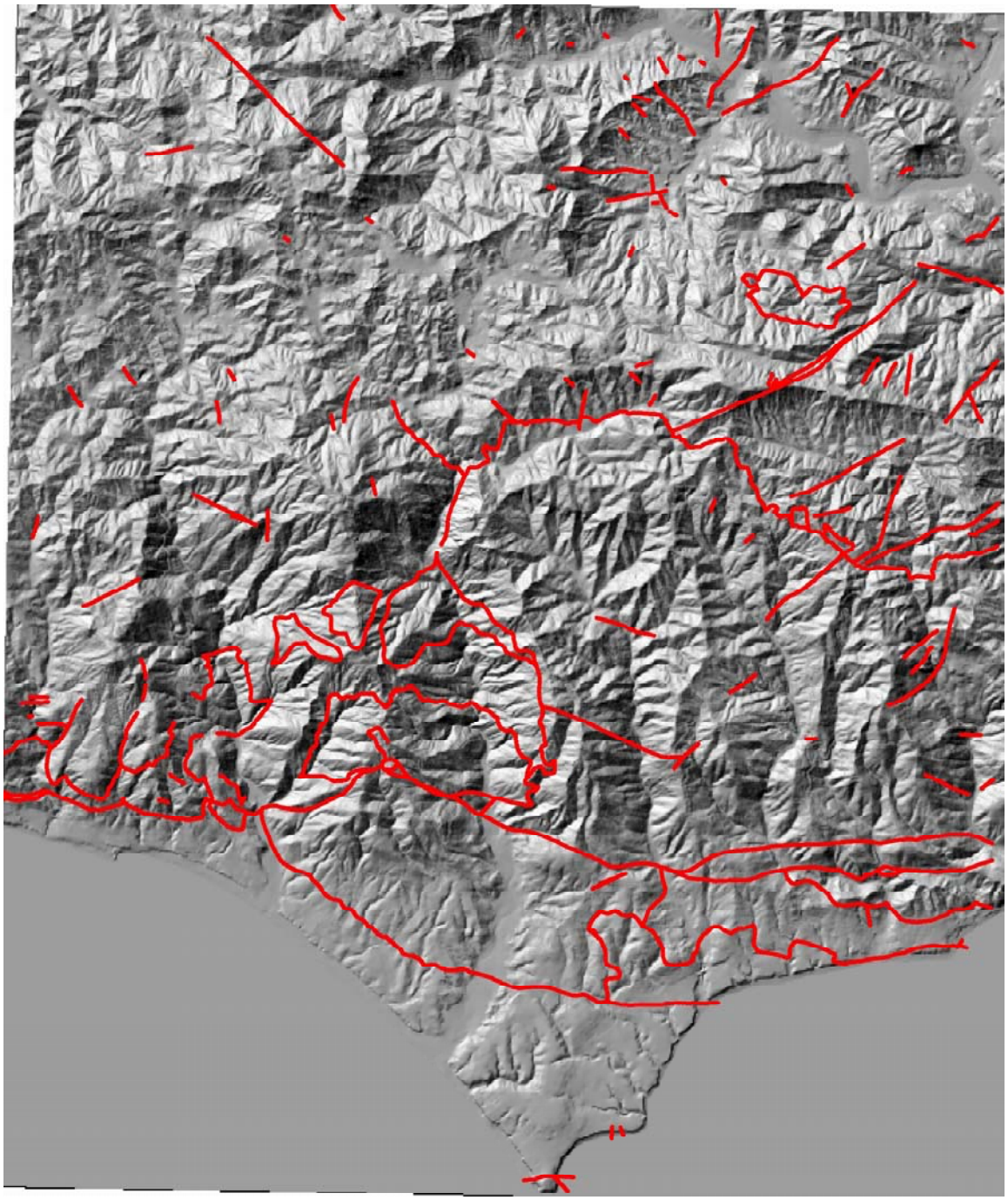

FIGURE 5. Map of current known faults (in red) within the Point Dume quadrangle, after Campbell and others (1996).

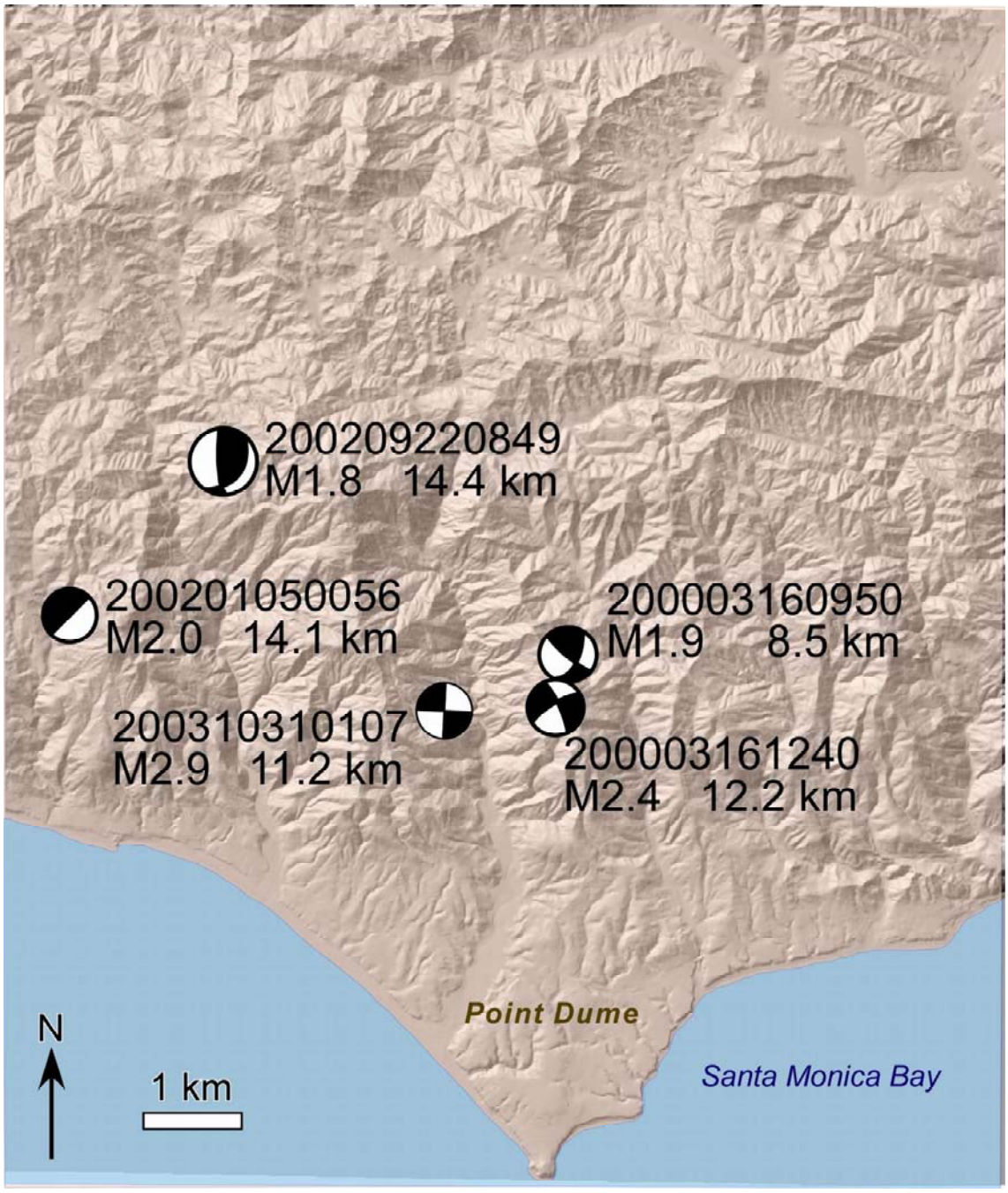

FIGURE 6. Earthquake epicenter locations for events with published focal mechanism solutions reported within the Point Dume 7.5 minute quadrangle. Data from Hauksson, (2004).

CHAPTER THREE

Methods

A set of published topographic and geologic maps of the Point Dume 7.5 minute quadrangle and vicinity was collected. The most important of these maps were the *Geologic map of the Point Dume quadrangle, Los Angeles County, California* (Campbell and others, 1996), *Geologic map of the Point Dume Quadrangle, Los Angeles County, California* (Dibblee and Ehrenspeck, 1993), and the *Geologic map of east-central Santa Monica Mountains, Los Angeles County, California* (Yerkes and Campbell, 1980). Digital data related to the USGS geologic mapping of the Point Dume Quadrangle are available at http://pubs.usgs.gov/of/1997/of97-276/ and http://geo-nsdi.er.usgs.gov/metadata/open-file/97-276/metadata.faq.html. Google Earth (http://earth.google.com/) was used to provide aerial photographic coverage of the study area. Digital elevation models (DEMs) created by the U.S. Geological Survey at 30-meter and 10-meter resolution were obtained from the Geocommunity web site (http://data.geocomm.com/).

Cronin has compiled an earthquake catalog including events with epicenters reported in the central or western Santa Monica Mountains and northern Santa Monica Bay (Cronin and Sverdrup, 1998; http://www3.baylor.edu/~Vince_Cronin/ MalibuCurrentEQFile.xls). This catalog contains many if not all of the published focal-mechanism solutions for earthquakes in this area of southern California, drawn from published papers, theses, and online datasets (*e.g.,* Buika and Teng, 1979; Hardebeck, 2005; Hauksson, 1990, 2000, 2004; Hauksson and Saldivar, 1986; Lee and others, 1979; Stierman and Ellsworth, 1976;

Webb and Kanamori, 1985). The earthquake data used in this thesis were drawn from this database.

Seismo-Lineament Analysis

Cronin has developed a method that uses data from earthquake focal-mechanism solutions to define the intersection of fault-plane solutions and a DEM of the ground surface (Cronin, personal communication, 2004). Projecting a fault-plane solution to the ground surface would yield a single curve marking the trace of that plane across the irregular ground surface. In its current form, Cronin's method takes into account the reported vertical and horizontal uncertainty in the location of the earthquake focus. Given this uncertainty, the intersection of the fault-plane solution and the DEM surface is a swath that defines the range of potential intersections of the two surfaces at a given confidence interval. This uncertainty swath is called a *seismo-lineament* (Cronin, personal communication, 2004).

As described by Cronin (unpublished manuscript, 2006; used here with permisison), the seismo-lineament is defined using the following input data: the location and location errors associated with an earthquake focus, the orientation of one of the two nodal planes from the focal-mechanism solution, and the rake of the associated slip vector. Rake is the angle between the slip vector and the reference strike of the fault, where the reference strike is determined by the right-hand rule. A positive rake is directed upward, indicating a component of reverse slip, while a negative rake indicates a component of normal slip.

The computations that define the seismo-lineament relative to a DEM are done using code written in *Mathematica* by Cronin (2004). The location of the earthquake focus is converted to UTM coordinates $\{x_{\text{focus}}, y_{\text{focus}}, z_{\text{focus}}\}$ as described by Snyder (1982, p. 63-69

and 233-235), where z_{focus} is the focal depth in meters relative to sea level. The sign of the z_{focus} value is negative if the focus was below sea level.

The first several records in the DEM contain header data that define the number of rows (*nrows*) and columns (*ncols*) in the matrix of elevation data, the UTM coordinates of the lower-left corner ($x_{llcorner}$, $y_{llcorner}$), the horizontal distance between adjacent elevation data (*cellsize*), and the value used to indicate "no data" within the matrix (Maune, 2001). The matrix of elevation data follows the header, with the horizontal coordinates of each elevation datum implied by its location within the matrix. The UTM coordinates of the datum in row i and column j of the matrix (where $i = 1$ for the first row of elevation data) are

$$x \text{ coordinate} = x_{llcorner} + ((cellsize)\,(j - 1)) \tag{1a}$$

$$y \text{ coordinate} = y_{llcorner} + ((cellsize)\,(nrows - i)). \tag{1b}$$

and the z coordinate (*i.e.*, the elevation) is the value that occupies position [i, j] of the matrix.

Data derived from the focal mechanism solution are used to define several vector quantities needed in the analysis. The unit vector along the fault dip (*dipVector*) is computed using the plunge and trend of the fault dip:

$$dipVector = \{\cos(\text{plunge})\sin(\text{trend}), \cos(\text{plunge})\cos(\text{trend}), -\sin(\text{plunge})\}. \tag{2}$$

The unit vector associated with the reference strike of the fault plane is

$$strikeVector = \{\sin(\text{trend} - 90°), \cos(\text{trend} - 90°), 0\}. \tag{3}$$

The unit vector normal to the fault plane (**N**) is defined by the vector cross product

$$\mathbf{N} = dipVector \times strikeVector. \tag{4}$$

The UTM coordinates associated with the DEM are transformed by rigid translation to a coordinate system whose origin is coincident with the earthquake focus. The transformed coordinates of the datum in row *i* and column *j* of the data matrix are

$$x_{(i,j)\text{trans}} = (\text{cellsize} * (j - 1)) + (x_{\text{llcorner}} - x_{\text{focus}}) \quad (5a)$$

$$y_{(i,j)\text{trans}} = (\text{cellsize} * (\text{nrows} - i)) + (y_{\text{llcorner}} - y_{\text{focus}}) \quad (5b)$$

$$z_{(i,j)\text{trans}} = \text{elevation}_{(i,j)} - z_{\text{focus}} \quad (5c)$$

where $\text{elevation}_{(i,j)}$ is the value in row *i*, column *j* of the original data matrix. The vector $\mathbf{L}_{i,j} = \{x_{(i,j)\text{trans}}, y_{(i,j)\text{trans}}, z_{(i,j)\text{trans}}\}$ is the location vector to the point at row *i* and column *j* of the transformed data matrix, relative to a coordinate-system in which the origin is coincident with the earthquake focus.

The distance between the fault plane and the point on the DEM surface associated with location vector $\mathbf{L}_{i,j}$, in meter units, is the result of the vector dot product

$$d_{i,j} = \mathbf{N} \bullet \mathbf{L}_{i,j} \quad (6)$$

(Figure 7a).

For a fault plane with a dip angle of δ passing through a focal point whose location is known plus-or-minus some vertical error (v_e in meters) and horizontal error (h_e in meters), the half-width of the uncertainty envelope (w_e) is given by

$$w_e = [v_e * \cos(\delta)] + [h_e * \sin(\delta)] \quad (7)$$

(Figure 7b). Any point on the DEM for which the distance to the reported fault plane is less than or equal to the half-width of the location uncertainty envelope is considered to lie within the seismo-lineament swath that will be the focus of field evaluation (Figure 8). The seismo-lineament swaths are incorporated in a GIS dataset to facilitate reconnaissance mapping.

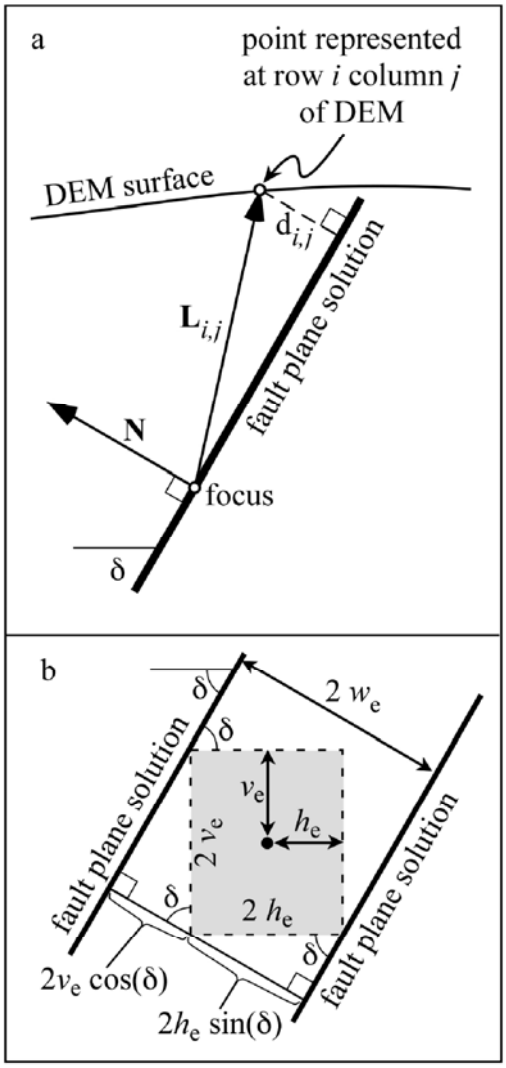

FIGURE 7. (a) Cross section showing geometry of vectors and fault plane used in this method. Angle δ is the fault dip, unit vector **N** is normal to the fault plane, location vector $\mathbf{L}_{i,j}$ is directed toward a point on the DEM surface that is $d_{i,j}$ meters away from the fault plane. (b) Cross section showing the uncertainty region (gray box) around the earthquake focus (black dot) bracketed by parallel fault-plane solutions. Angle δ is the dip angle of the model fault, v_e is the uncertainty in focal depth, h_e is the horizontal uncertainty in focal location, w_e is the half width of the uncertainty envelope between the fault planes. This figure is copyright (2006) by Cronin and is used with permission.

The vertical uncertainty region for some focal-location solutions extends above the ground surface or below the nominal seismogenic zone that is characteristic of a given area.

Constraint is imposed so that only focal locations within the statistical estimate of uncertainty that are below the ground surface are used to define the seismo-lineament

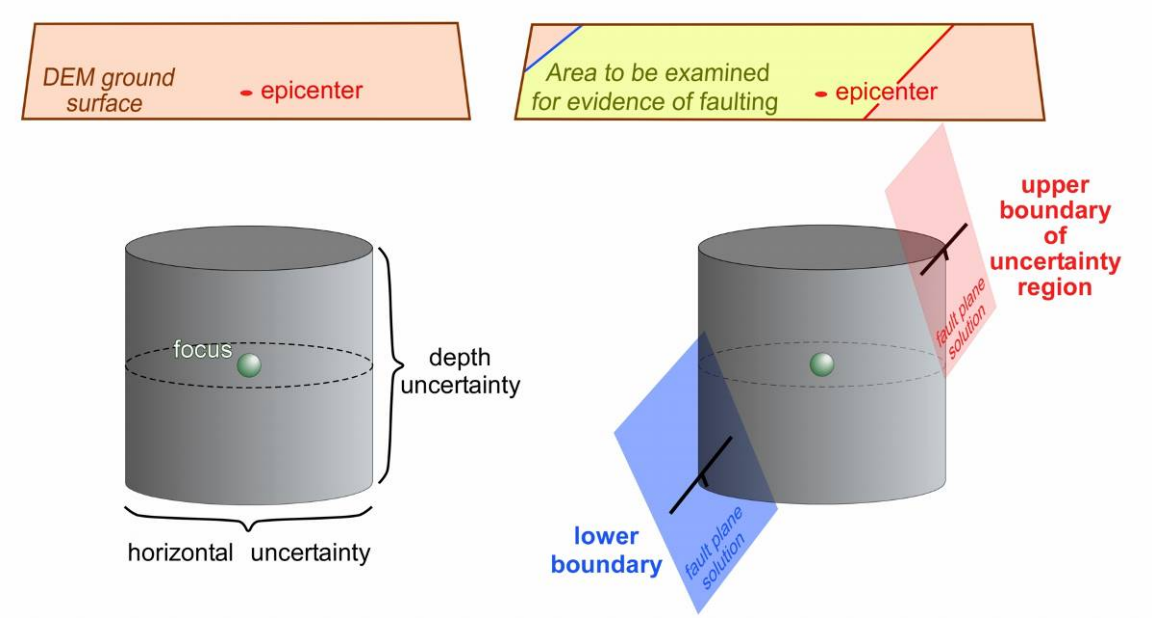

FIGURE 8. Three-dimensional visualization of how the seismo-lineament swath is bound by projected fault planes extending from opposite corners of the uncertainty region around the earthquake focus.

swath. An additional constraint may be imposed that requires focal locations to be within the statistical estimate of uncertainty *and* within the locally-defined seismogenic layer, if the depth of that layer can be reliably estimated based upon a sufficient historical record of well-located foci.

Each earthquake focal mechanism solution has two nodal planes, and so potentially generates two seismo-lineament swaths to be investigated (*e.g.*, Figure 9). In practice, one or both of the auxiliary planes for an event within the study area may not intersect the ground surface within the study area. The ground-surface area along the seismo-lineament

swaths is examined to identify any faults that may correlate with the specific earthquake. It would normally be expected that a fault would be evident along the trace of one of the

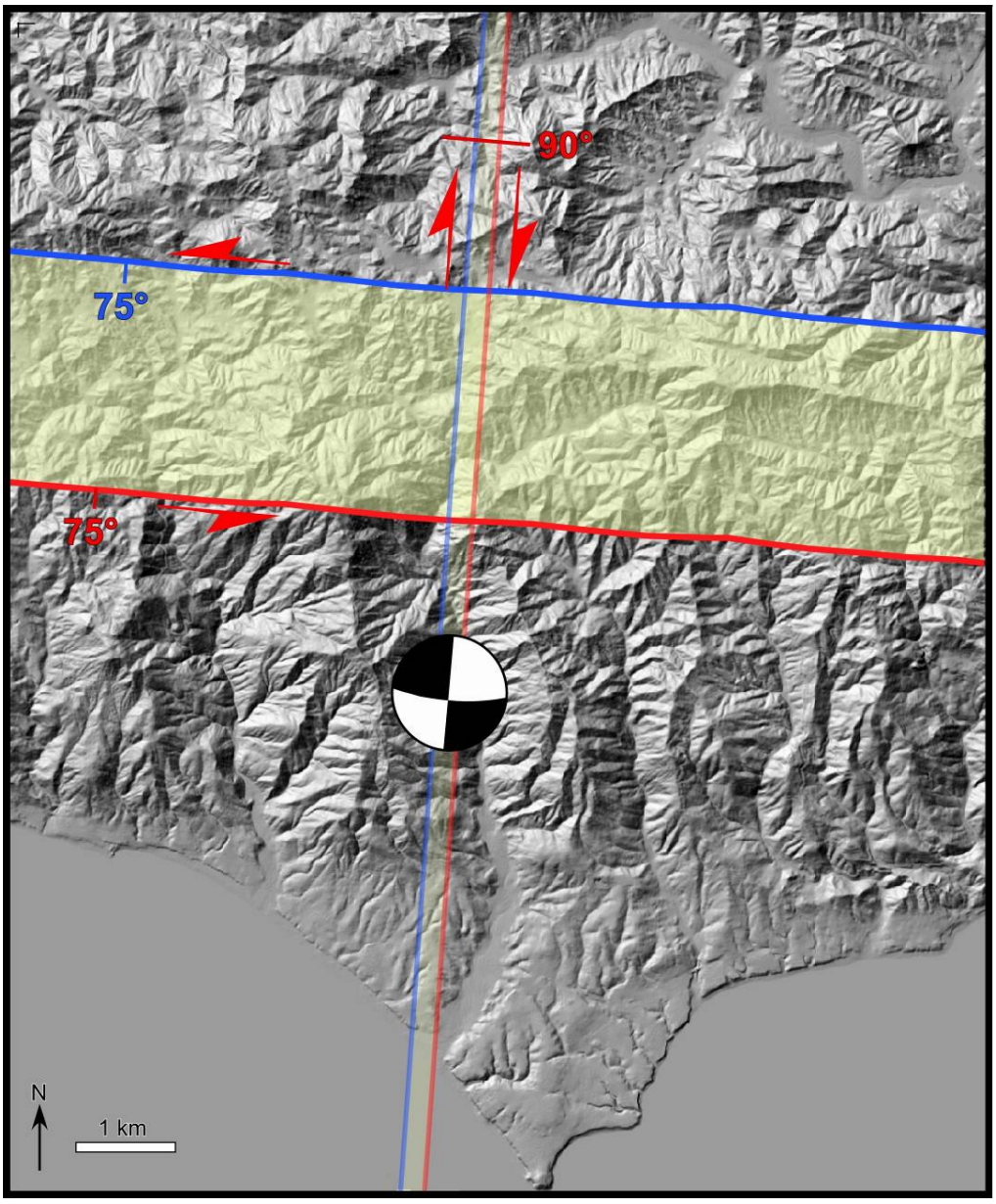

FIGURE 9. Surface trace of projected error regions for both nodal planes of a M2.9 earthquake recorded on October 31, 2003, at a depth of 11.2 km. Within one of the two yellow swaths may be found the surface trace of the fault along which the earthquake occurred. Focal mechanism solution is from Hauksson (2004).

nodal planes (*i.e.*, along the fault-plane solution), while no faulting would be evident along the other nodal plane (the auxiliary plane).

Geomorphic Lineaments

In their study of lineaments near the Nanga Parbat-Haramosh Massif of the northwest Himalaya, Cronin and others (1994, p. 196) stated "In this paper, the term lineament is used to describe a long (generally ≥ 5 km) colinear or slightly curving array of stream drainage segments or tonal boundaries within the Landsat mosaic that does not appear to be related to human construction or other [human] activities." Explicit in this definition of the word "lineament" is the length scale at which a lineament is to be defined. In our studies at Malibu, there seem to be at least two natural scales at which we might define lineaments. Most of the lineaments defined by criteria listed in the previous section will be on the order of 0.5 to 2 km in length, and we will refer to these as *local lineaments*. Several of these lineaments may define a longer, *composite lineament* that may extend for tens of kilometers. Operationally, it is preferred to begin by systematically identifying the local lineaments, and then use approximately colinear sets of local lineaments to define composite lineaments.

Some geomorphic features that are frequently developed along faults include (Wesson and others, 1975; Cronin and others, 1994; McCalpin 1996; Burbank and Anderson, 2001; Cronin, unpublished manuscript, 2006):

a. stream channels aligned across a drainage divide.

b. lower-order (smaller) stream channels aligned across a higher-order stream channel.

c. anomalously straight segment of a stream channel.

d. aligned straight segments of a stream channel.

e. lower-order stream channel whose trend is directed upstream relative to the higher-order stream it intersects, so water flowing from the smaller stream into the larger stream has to change directions through an acute angle.

f. abrupt changes in gradient along a stream channel.

(1) stream channel steps down in direction of flow, evinced by rapids or a waterfall (knick point).

(2) stream channel steps up in direction of flow, evinced by a pond.

g. apparent lateral deflection of an incised stream channel or flood plain.

h. abrupt changes in gradient along a ridge crest.

(1) ridge crest steps down abruptly in the direction the ridge is decreasing in elevation.

(2) ridge crest steps up in the direction the ridge is decreasing in elevation.

(3) a saddle in the ridge crest.

i. apparent lateral deflection of a ridge crest.

j. abrupt changes in the gradient of a surface localized along a narrow linear step (fault scarp).

k. benches or faceted spurs at the base of ridges that are unrelated to coastal erosion.

l. a set of ridges in an *en echelon* array.

m. a topographic basin along a linear trough (pull-apart basin, sag pond).

n. a topographic hill along a linear trough (pop-up, pressure ridge).

o. a ridge across the mouth of a stream drainage that is not a glacial moraine (shutter ridge).

The geomorphic signature of the Malibu Coast Fault is clearly recorded on aerial photographs (*e.g.,* Figure 10).

In addition to the foregoing list of features, which can be discerned on a DEM of suitable resolution using only information about the shape of the ground surface, other features that may be related to faults can be recognized on aerial photographs or on imagery produced using sensors from satellites like Landsat and SPOT (Cronin, unpublished manuscript, 2006). These include:

a. linear boundaries in vegetation.

b. linear boundaries in soil type as indicated by different spectral reflectance.

FIGURE 10. Example of a high resolution aerial photograph of the Malibu coastline showing Big Rock Mesa and southern Las Flores Canyon, with the inferred trace of the Malibu Coast Fault (Yerkes and Wentworth, 1965) bracketed between the yellow lines.

c. linear arrays of vegetation or soil, developed because of local changes in soil moisture.

d. variations in vegetative health or density along a linear trend.

e. linear arrays of springs, as water flow from subsurface to surface is controlled by some geologic boundary.

f. linear concentrations of landslides, as slopes adjacent to a fault zone are fractured and fail.

g. linear boundaries in the general tone or texture of the imaged surface -- features that result from the combined influences of soil, rock, slope and vegetation, neglecting human influences.

In this research project, geomorphic analysis intended to define lineaments that may have developed along faults was conducted primarily with a 10-meter DEM, visualized using either ArcGIS or Guth's application MicroDEM (http://www.usna.edu/Users/oceano/pguth/website/microdem.htm). One advantage that a DEM has over an aerial photograph is that the DEM contains only information about the shape of the ground surface, and is largely devoid of human-related artifacts (*e.g.,* structures, roads, grading scars) that can distract an interpreter. Another significant advantage is that an aerial photograph has a fixed direction of illumination: always from the southern half of the compass rose, whereas a DEM can be artificially illuminated from any direction. An image of the DEM surface was illuminated from an elevation of 45° and from various azimuths in order to accentuate linear geomorphic features that are represented in the DEM (*e.g.,* Figure 11).

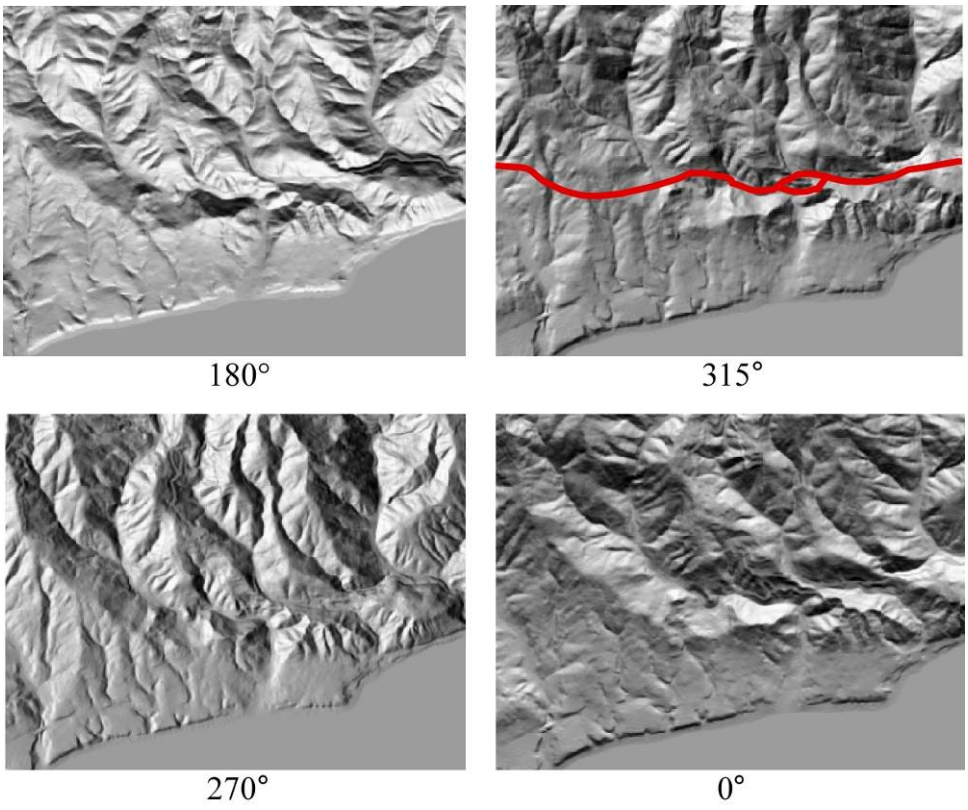

FIGURE 11. A portion of the Point Dume DEM, showing the mapped trace of the Malibu Coast Fault (in red) and the geomorphic lineament which it produces, indicated by visible offset of streams. Illumination azimuths are noted at the base of each. Malibu Coast Fault is depicted in red (Yerkes and Wentworth, 1965).

Field Methods

The seismo-lineament analysis and the geomorphic analysis result in the development of a set of hypotheses concerning locations where seismogenic faults may be found at the surface. These hypotheses are tested by going to locations where the seismo-lineaments cross a road or trail and look for evidence of faulting.

Each earthquake generates two seismo-lineament swaths to be investigated. The ground-surface area along the seismo-lineament swaths is examined to identify any faults that may correlate with the earthquake. During initial reconnaissance, two attributes of a

fault observed within the seismo-lineament swath are used to tentatively correlate the fault with the earthquake: the fault-surface orientation and the orientation of slip-direction indicators along the fault.

Active brittle faults exposed at the ground surface typically feature a zone of fault rock (*e.g.,* gouge, breccia, cataclasite) bounded by sub-parallel shear-smoothed surfaces, beyond which is a damage zone within the local bedrock (Chester and others, 2004). Multiple measurements of the orientation of the fault-bounding surfaces are collected using a field compass with a clinometer.

The orientation of shear-related grooves and striations are recorded by measuring the rake of the shear lineation (fig. 12). If the hanging-wall slip direction can be determined unambiguously in the field, the shear lineation is treated as a unit-vector quantity; otherwise, the investigator explicitly notes that one direction along the lineation has been arbitrarily chosen for measurement -- usually the "down" direction in accordance with traditional geological practice. Oriented specimens along the fault surface are collected to establish or verify the sense of slip. The rake of the slip vector is measured relative to the reference strike of the fault surface, which is defined by an anti-clockwise (right-handed) rotation from the fault's dip vector. A positive rake for a hanging-wall slip vector indicates a reverse component of motion. The site mean orientation and the radius of the 95% confidence interval are computed for both the fault surface and the slip vectors using Fisher statistics (Cronin, 2007).

To summarize, the following data are collected where there is evidence of faulting:

a. location of the fault, using GPS and traditional mapping on a topographic base.

b. photographs.

FIGURE 12. Example of slickenside with prominent striations. The orientations of the slickenlines were measured to obtain a rake vector. Note the pencil for scale.

c. measurement of the width of gouge zones.

d. oriented samples of rock in the damage zone adjacent to the gouge zone.

e. samples of the gouge zone.

f. a statistically relevant number of measurements of the orientation of the sides of the gouge zone.

g. a statistically relevant number of measurements of the orientation of grooves or scratches related to fault shear, and so on.

h. a general description of the rock units adjacent to the fault at that location.

i. any information that may help constrain the direction or the amount of slip.

CHAPTER FOUR

Results

Geomorphic Lineaments

The summary map of geomorphic lineaments is presented as Figure 13. There appear to be 3 prominent trends: east, east-northeast and west-northwest. Some of the lineaments correlate with previously mapped faults.

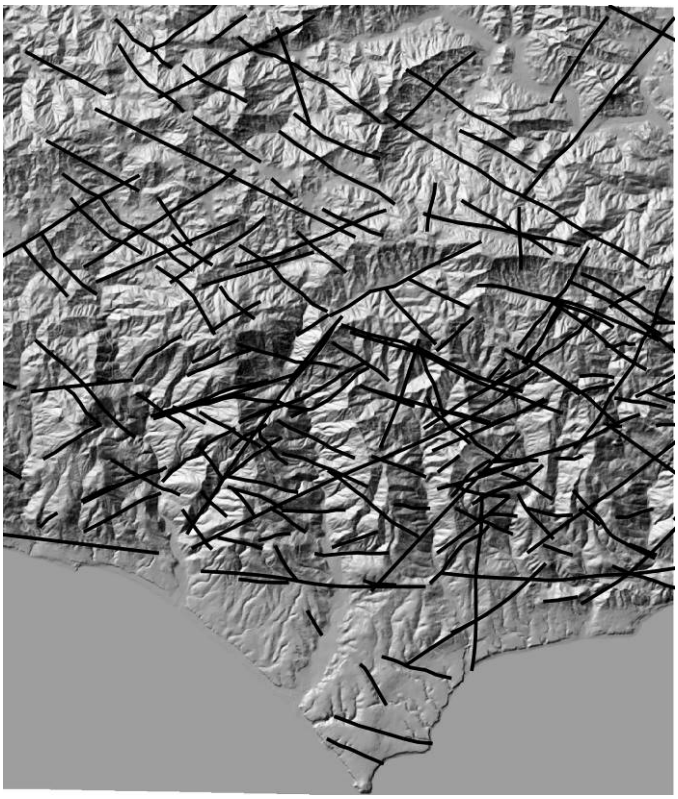

FIGURE 13. Geomorphic lineament map of the Point Dume quadrangle. This figure shows a general pattern in the structural fabric.

Seismo-Lineaments

The maps of seismo-lineaments generated using Cronin's *Mathematica* code were plotted in ArcGIS. Focal mechanism solutions from eight different earthquakes were used in this study. Two earthquakes had both nodal planes that intersected the ground surface within the study area, four had just one plane in the field area, and the remaining two had nodal planes that did not project into the field area (fig. 14).

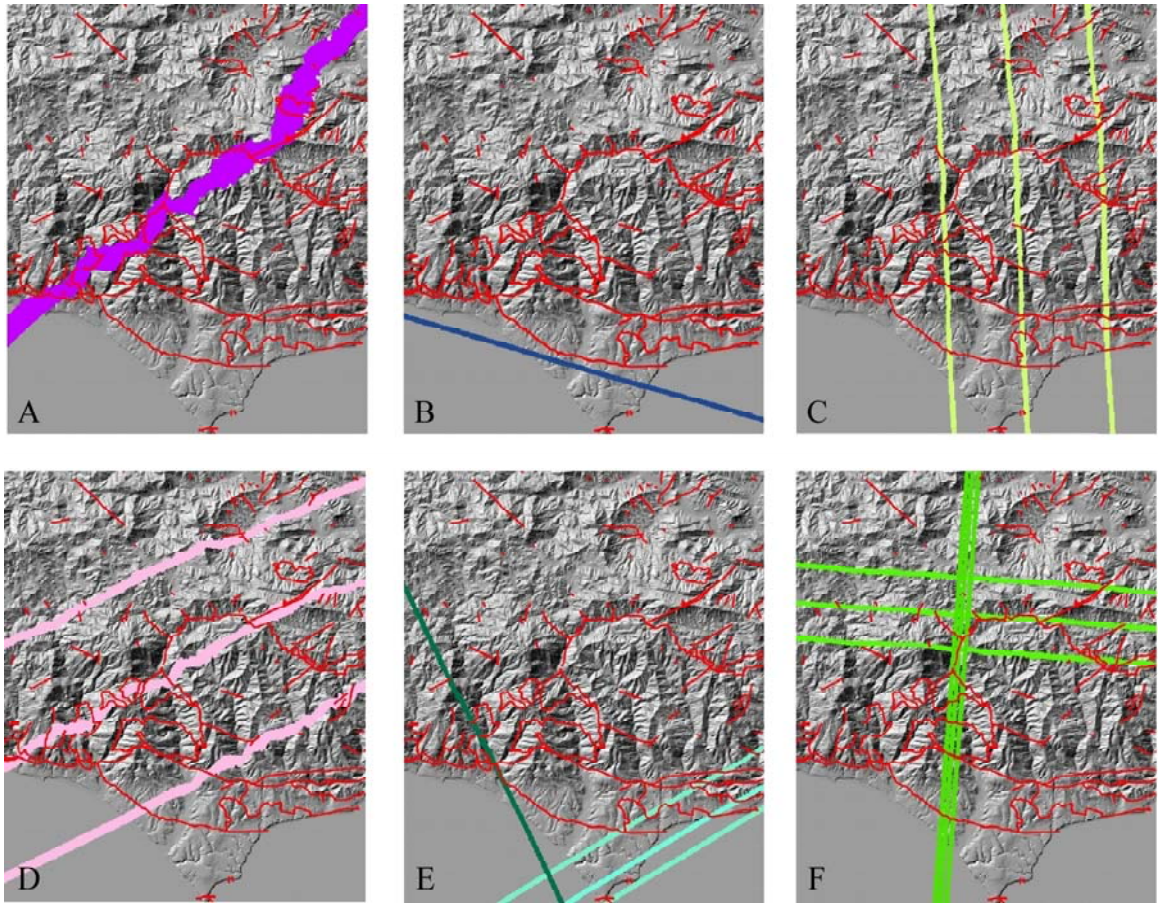

FIGURE 14. Maps showing seismo-lineaments generated by the projection of focal mechanism nodal planes. Seismo-lineament maps were generated using *Mathematica* and plotted as shown using ArcGIS. (A) Seismo-lineament for the M3.3 earthquake on September 16, 2000. (B) Seismo-lineament for the M2.7 earthquake on July 14, 1972. (C) Seismo-lineament for the M1.8 earthquake on November 12, 2002. (D) Seismo-lineament for the M2.0 earthquake on July 30, 2000. (E) Seismo-lineament for the M2.4 earthquake on March 16, 2000. (F) Seismo-lineaments (both nodal planes) for the M2.9 event on October 31, 2003.

Field Site Observations

Faults which corresponded to the seismo-lineaments are generally located in roadcuts in highland areas (fig. 15). All GPS coordinates were recorded in latitude/longitude format using the North American datum of 1927.

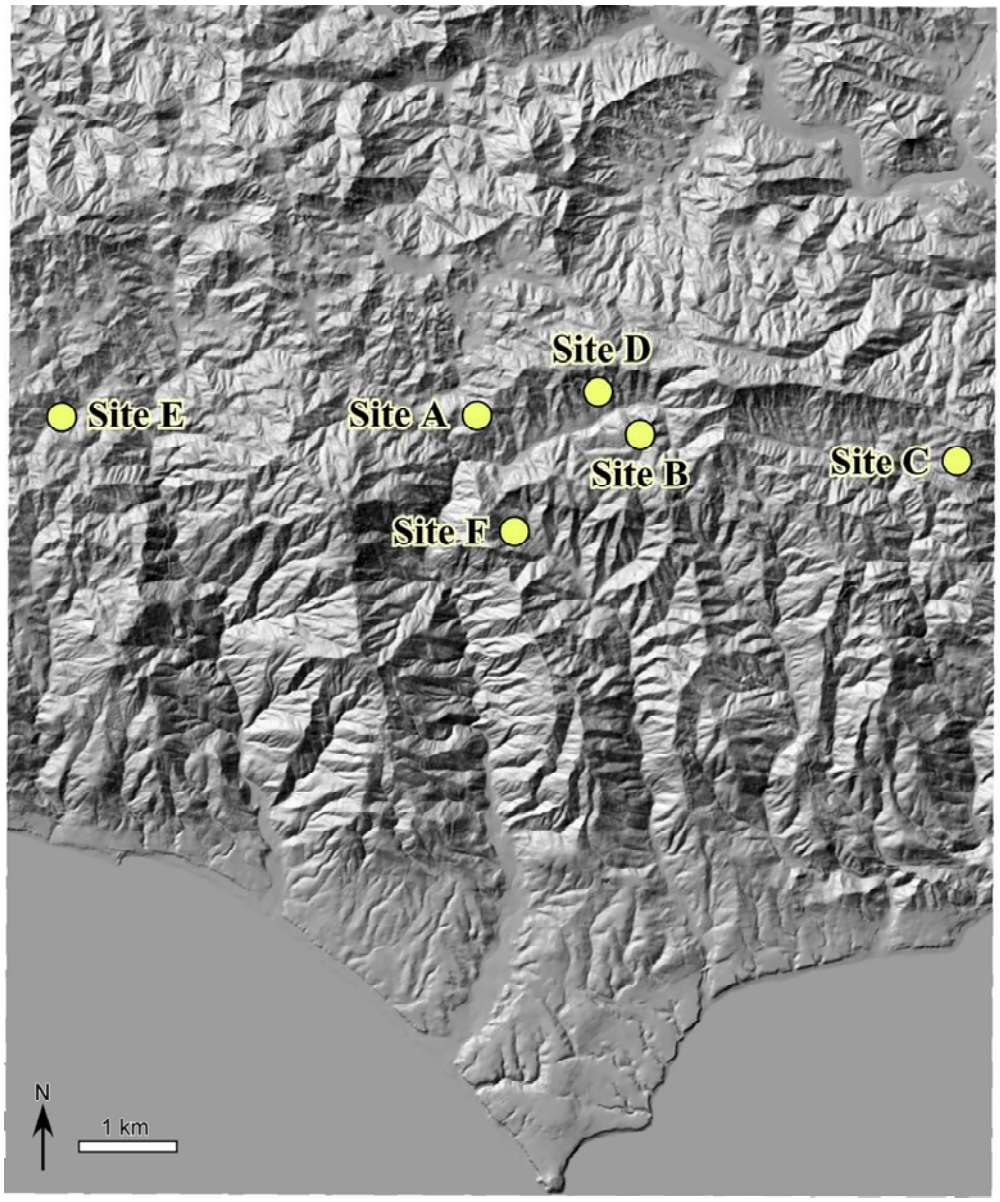

FIGURE 15. DEM of the Point Dume quad showing approximate locations of each outcrop where a previously unmapped fault was identified.

Site A is located at latitude N34° 05’ 14.2”, longitude W118° 48’ 57.4”, with an uncertainty of 15 feet. The elevation was 1,754 feet with an uncertainty of 23 feet. The outcrop is located within the error region for an M 2.9 earthquake that occurred on October 31, 2003 (Hauksson, 2004). Its reported epicenter was located at latitude 34.0562 and longitude -118.8212, with a horizontal uncertainty of 0.2 km. The reported depth was 11.18 km, with a vertical uncertainty of 28.1 km. The reported fault plane solution has a dip azimuth of 185°, dip angle of 75°, and rake of 0°; the other nodal plane has a dip azimuth of 95°, dip angle of 90°, and rake of 165°.

The lithology of the intact rock on either side of this fault is a coarse grained tan sandstone of the lower Topanga Formation, which is gently dipping to the north (fig. 16). The fault rock is a tan non-cohesive fault gouge (fig. 17). Chips with surfaces containing shear striations (slickensides) were observed within the fault gouge; however, a sense of slip could not be determined due to the incohesive nature of the gouge. The fault’s mean dip vector plunges 6° toward 80° azimuth, with a 95% confidence interval of ±2°. This is a previously unmapped fault.

Site B is located at latitude N34° 04’ 47.5”, longitude W118° 45’ 18.8”, with an uncertainty of 15 feet. The elevation was 1981 feet with an uncertainty of 23 feet. The outcrop is located within the error region for an M 2.9 earthquake that occurred on October 31, 2003 (Hauksson, 2004). Its reported epicenter was located at latitude 34.0562 and longitude -118.8212, with a horizontal uncertainty of 0.2 km. The reported depth was 11.18 km, with a vertical uncertainty of 28.1 km. The reported fault plane solution has a dip azimuth of 185°, dip angle of 75°, and rake of 0°.

FIGURE 16. Fault at site A, an uninterpreted photograph at top. The same photo below with fault interpretation. Black lines indicate the edge of the fault zone. Fault is approximately 2 meters wide.

FIGURE 17. Detail view of fault at site A, showing the fault gouge and shear surfaces, The gouge zone is two meters wide.

The intact rock surrounding the fault zone is light tan coarse grained sandstone of the Sespe Formation, which dips steeply to the north (fig. 18). The southern edge of the fault at this location appears to be an igneous intrusion. The fault's mean dip vector plunges 73° toward 28° azimuth, with a 95% confidence interval of ±9°. This is a previously unmapped fault.

Site C is located at latitude N34° 04' 57.2", longitude W118° 45' 43.5", with an uncertainty of 18 feet. The elevation was 1,832 feet with an uncertainty of 27 feet. The outcrop is located within the error region for an M 2.9 earthquake that occurred on October 31, 2003 (Hauksson, 2004). Its reported epicenter was located at latitude 34.0562 and longitude -118.8212, with a horizontal uncertainty of 0.2 km. The reported depth was

FIGURE 18. Fault at site B, an uninterpreted photograph at top. The same photo below with fault interpretation. Black lines indicate the edge of the fault zone. Note shovel for scale.

11.18 km, with a vertical uncertainty of 28.1 km. The reported fault plane solution has a dip azimuth of 185°, dip angle of 75°, and rake of 0°.

The surrounding rock is white sandstone of the Sespe Formation. The southern edge of the fault is partially covered by debris from a small landslide (fig. 19). The fault is ~1 meter wide, and is characterized by pulverized rock with slickensides developed on some semi-cohesive clumps of gouge. The fault's mean dip vector plunges 76° toward 359° azimuth, with a 95% confidence interval of ±5°. This is a previously unmapped fault.

Site D is located at latitude N34° 05' 02.8", longitude W118° 47' 43.5", with an uncertainty of 19 feet (fig. 20). The elevation was 1,951 feet with an uncertainty of 28 feet. The outcrop is located within the error region for an M 2.0 earthquake that occurred on July 30, 2000 (Hauksson, 2004). Its reported epicenter was located at latitude 34.1125 and longitude -118.5317, with a horizontal uncertainty of 0.2 km. The reported depth was 0.2 km, with a vertical uncertainty of 3.2 km. The reported fault plane solution has a dip azimuth of 155°, dip angle of 45°, and rake of -20°; the other nodal plane has a dip azimuth of 259°, dip angle of 76°, and rake of -133°.

The surrounding rock is interbedded brown sandstone and siltsone of the Vaqueros Formation (lower Topanga), and is dipping gently to the north. The width of the fault is ~1 meter. The fault zone is characterized by pulverized rock with slickensides developed on some semi-cohesive clumps of gouge. Faint horizontal shear striae are present on some of the gouge material and on the fault walls. The fault's mean dip vector plunges 84° toward 326° azimuth, with a 95% confidence interval of ±27°. This is a previously unmapped fault.

FIGURE 19. Fault at site C, an uninterpreted photograph at top. The same photo below with fault interpretation. Black lines indicate the edge of the fault zone. Note shovel for scale.

FIGURE 20. Fault at site D, an uninterpreted photograph at top. The same photo below with fault interpretation. Black lines indicate the edge of the fault zone.

Site E is located at latitude N34° 04’ 54.0”, longitude W118° 52’ 18.9”, with an uncertainty of 25 feet (fig. 21). The elevation was 1,391 feet with an uncertainty of 38 feet. The outcrop is located within the error region for an M 2.4 earthquake that occurred on March 16, 2000 (Hauksson, 2004). Its reported epicenter was located at latitude 34.0488 and longitude -118.8092, with a horizontal uncertainty of 0.3 km. The reported depth was 12.18 km, with a vertical uncertainty of 2.4 km. The reported fault plane solution has a dip azimuth of 65°, dip angle of 75°, and rake of -160°; the other nodal plane has a dip azimuth of 330°, dip angle of 71°, and rake of -16°.

The surrounding rock is comprised of mafic volcanics and brown sandstones of the Conejo Volcanic Formation. The width of the fault is ~1 meter. The fault is observed in roadcuts on both sides of the road. The fault zone is characterized by pulverized rock with slickensides developed on some semi-cohesive clumps of gouge. Faint horizontal shear striae are present on some of the gouge material, indicating a horizontal sense of slip. The fault’s mean dip vector plunges 77° toward 65° azimuth, with a 95% confidence interval of ±5°. This is a previously unmapped fault.

Site F is located at latitude N34° 04’ 14.4”, longitude W118° 48’ 43.1”, with an uncertainty of 28 feet (fig. 22). The elevation was 1,510 feet with an uncertainty of 42 feet. Large slickensides at various orientations are present. The surrounding rocks are volcanic pebble conglomerate or breccias of the Conejo Volcanic Formation. The presence of some non-parallel sets of shear striae along some sheared surfaces indicates that there have been several past movements. Banded mineralization of quartz and calcite are present along the fault, indicating fluid flow during movement.

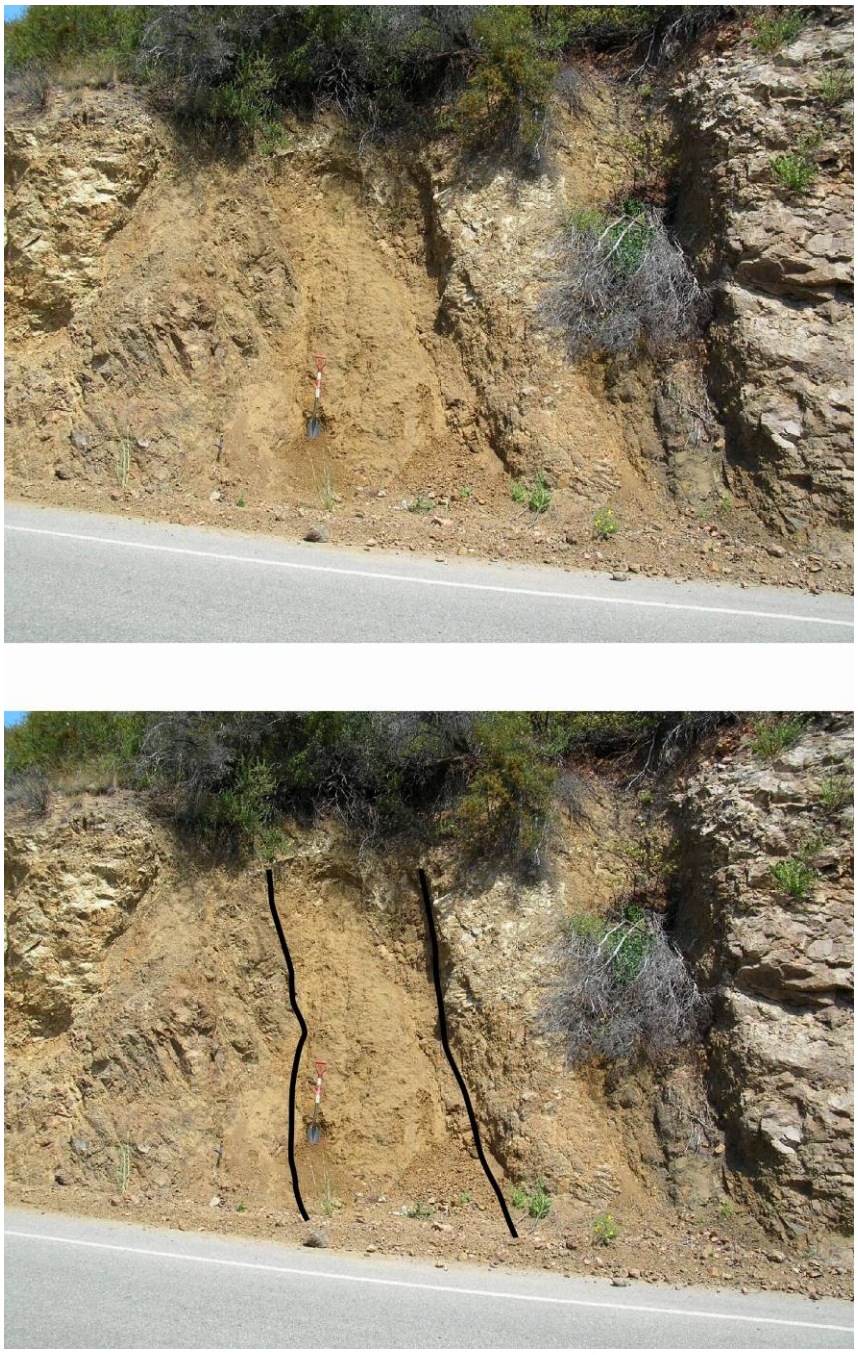

FIGURE 21. Fault at site E, an uninterpreted photograph at top. The same photo below with fault interpretation. Black lines indicate the edge of the fault zone. Note shovel for scale.

FIGURE 22. Site F, A view of a previously unmapped fault, which was identified during this study but does not correlate with any the study's current seismo-lineaments. Note vehicle for scale.

The outcrop is located within the error region for an M 2.9 earthquake that occurred on October 31, 2003; however, the orientation of this fault does not correlate with this particular earthquake or any of our other current seismo-lineaments. The fault's mean dip vector plunges 69° toward 44° azimuth, with a 95% confidence interval of ±4°. This is a previously unmapped fault.

Figure 23 shows the locations of outcrops where previously unmapped faults were identified within the seismo-lineament associated with the M 2.9 earthquake of October 31, 2003. These three faults have similar orientations, and their orientation and slip characteristics are similar to those of the projected nodal plane. Figure 24 shows the seismo-lineament associated with the M 2.0 earthquake of July 30, 2000, and the outcrop at Site D that includes a fault that appears to correlate with that earthquake. Figure 25 shows the seismo-lineament associated with the M 2.4 earthquake of March 16, 2000, and the outcrop at Site E that includes a fault that appears to correlate with that earthquake.

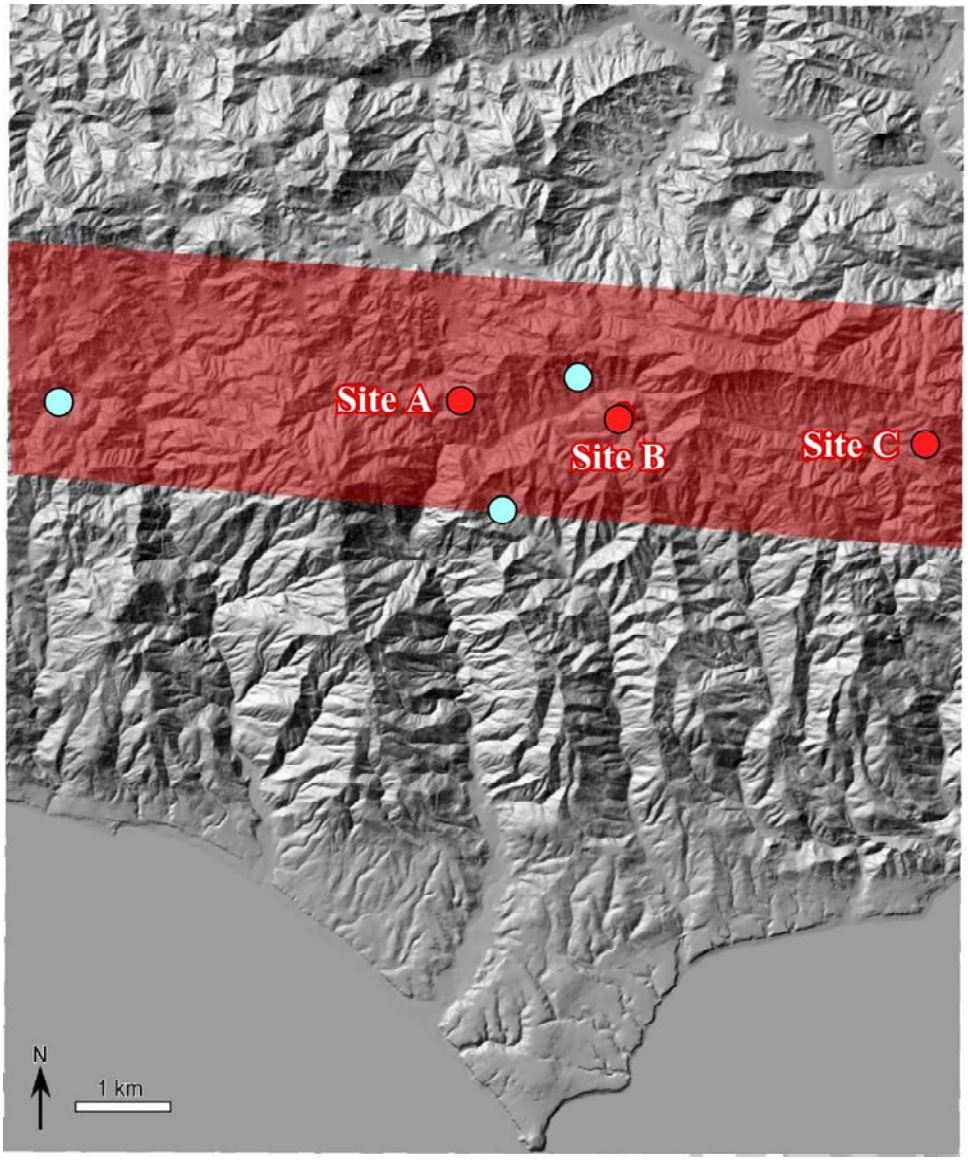

FIGURE 23. DEM of the Point Dume quad showing (in red) seismo-lineament for the M 2.9 earthquake of October 31, 2003. The red dots represent the locations of outcrops where previously unmapped faults were found that have similar slip characteristics to the earthquake. The blue dots represent outcrops with other previously unmapped faults, two of which correlate to another seismo-lineaments.

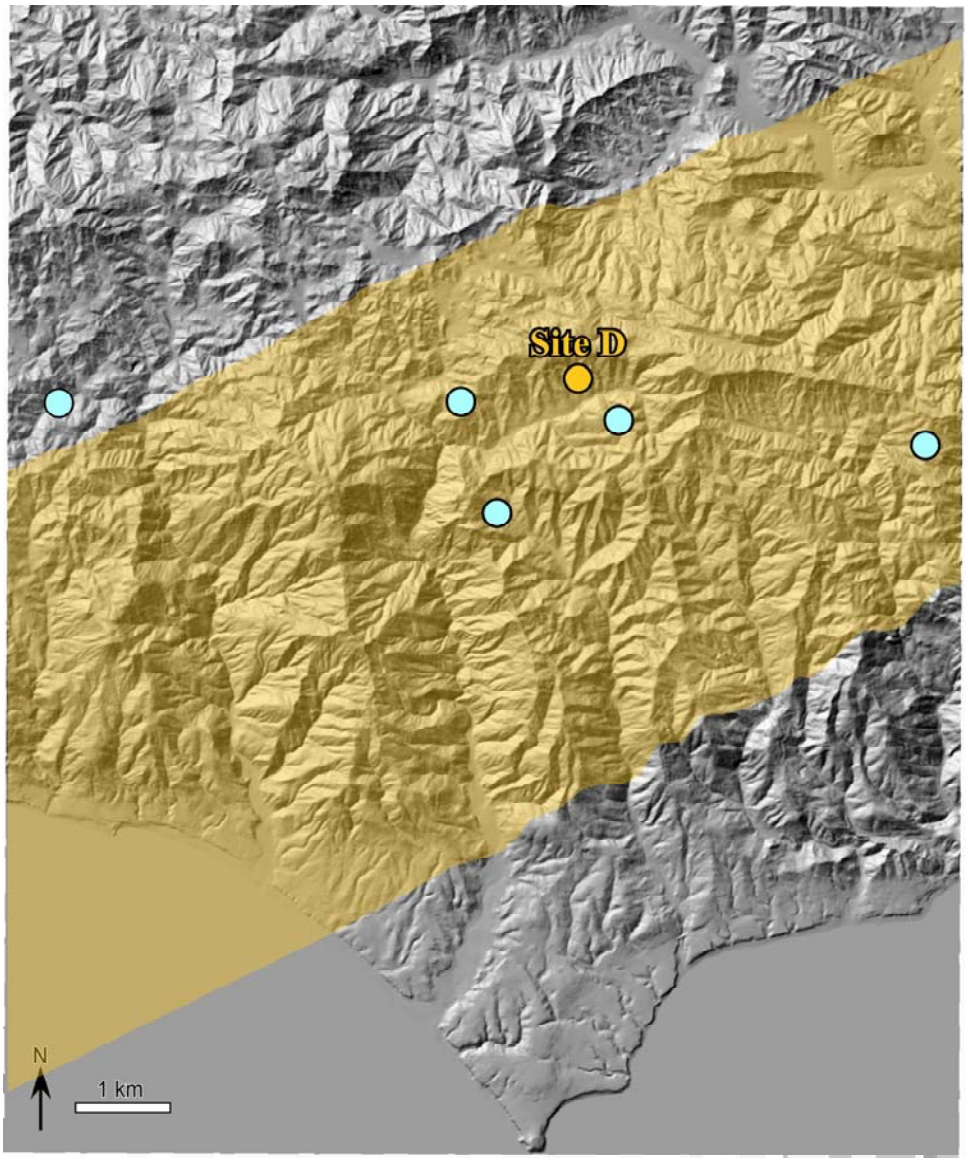

FIGURE 24. DEM of the Point Dume quad showing (in amber) seismo-lineament for the M 2.0 earthquake of July 30, 2000. The amber dot represents the location of the outcrop where a previously unmapped fault was found that has similar slip characteristics to the earthquake. The blue dots represent other outcrops with previously unmapped faults.

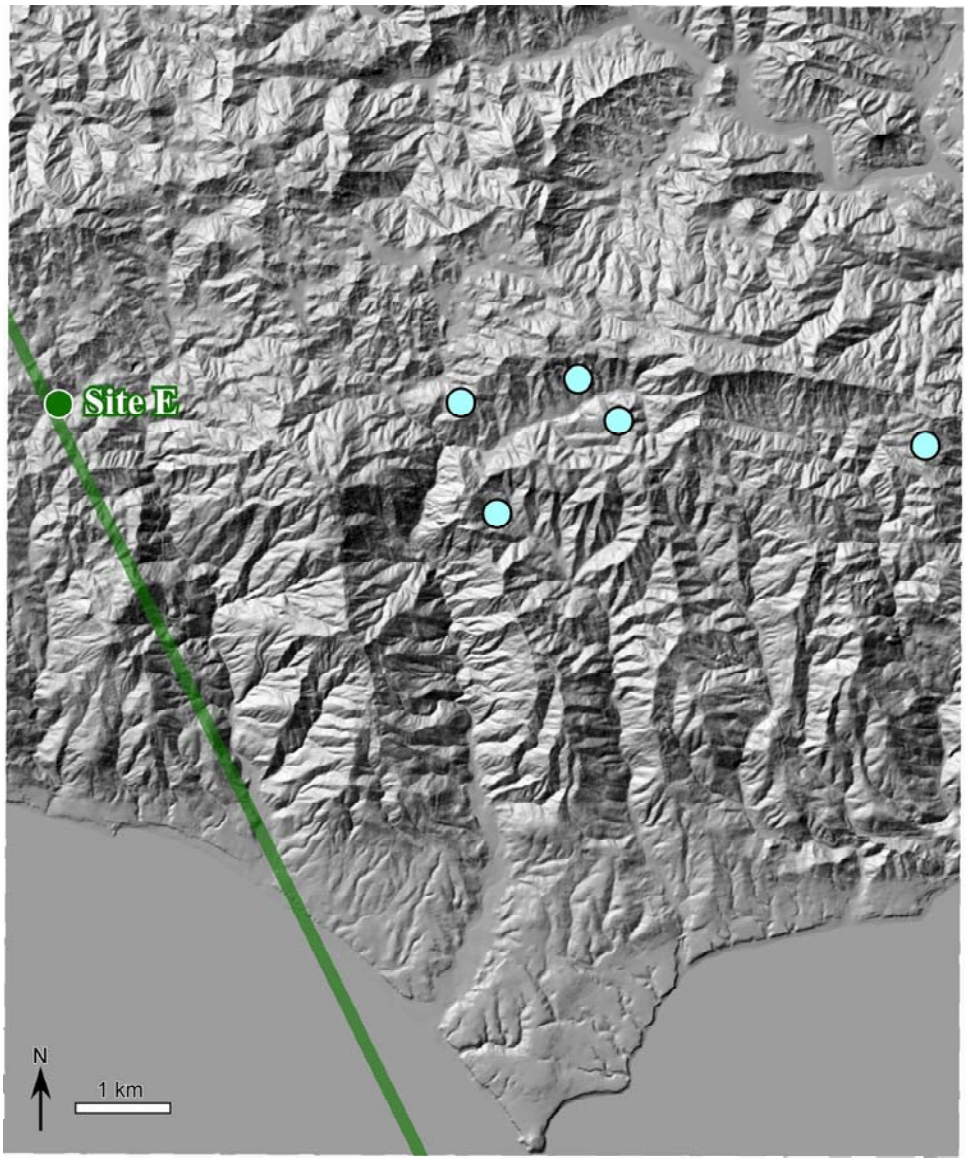

FIGURE 25. DEM of the Point Dume quad showing (in green) seismo-lineament for the M 2.4 earthquake of March 16, 2000. The green dot represents the locations of the outcrop where a previously unmapped fault was found that has similar slip characteristics to the earthquake. The blue dots represent other outcrops with previously unmapped faults.

CHAPTER FIVE

Discussion and Conclusions

The purpose of this thesis research is to test the idea of using seismo-lineaments to find potentially seismogenic faults – faults within the seismo-lineament that have approximately the same orientation and slip characteristics as the fault-plane solution that defined the corresponding seismo-lineament.

The seismo-lineament method for locating faults has resulted in the identification of several previously unmapped faults. Of these previously unmapped faults, three (sites A, B and C) may correlate with a recorded earthquake for which a focal-mechanism solution has been published: the M 2.9 earthquake of October 31, 2003 (fig. 23). These faults are located within a seismo-lineament swath associated with that earthquake, and they display orientations and slip characteristics that are generally consistent with that earthquake. Furthermore, there is a set of geomorphic lineaments that are within the seismo-lineament swath and trend approximately parallel to the swath boundaries. We infer that these faulted outcrops are associated with the same fault (perhaps on separate sub-parallel strands), and that it is a seismogenic, left-lateral strike-slip fault.

Two other previously-unmapped faults (sites D and E) were correlated to other earthquake events. A prominent, previously unmapped fault that is not related to any of the earthquakes used in this study was also identified (site F).

In the two cases where both nodal planes projected onto the ground surface within the study area, evidence of faulting was found in one (and only one) of the seismo-lineaments

each time. That is as one would predict, given that one of the nodal planes in a focal-mechanism solution corresponds to the orientation of the fault that produced the earthquake, while the other nodal plane (*i.e.,* the auxiliary plane) is not associated with any faulting.

The newly discovered faults will require additional study to evaluate whether they are active. Their surface trace should be mapped on the ground, with special attention paid to any accessible low spot or depocenters along their trend where a trench might be established. Procedures for evaluating fault activity using trenches are given by McCalpin (1996); however, such studies are beyond my technical expertise, and must be done by a geologist licensed by the State of California.

The interpretation of a strike-slip fault near the crest of the Santa Monica Mountains leads to a new ideas about the evolution of the mountain range. Strain partitioning, in which horizontal displacement occurs along a near-vertical fault and reverse displacement occurs along a low-angle thrust fault, is common in areas of oblique convergence (*e.g.,* Beck, 1983, 1984). Studies conducted in the Channel Islands, due west of the Santa Monica Mountains, suggest a partitioning of strain between thrust faults and strike-slip faults in the area (fig. 26; Legg and others, 2004). This type of situation may also be occurring in the Santa Monica Mountains. Applying the model of Legg and others (2004) to the Santa Monica Mountains, strain is partitioned between thrusting along the Malibu Coast Fault Zone (Malibu Coast fault, Anacapa-Dume faults) and strike-slip displacement along the newly identified fault (fig. 27).

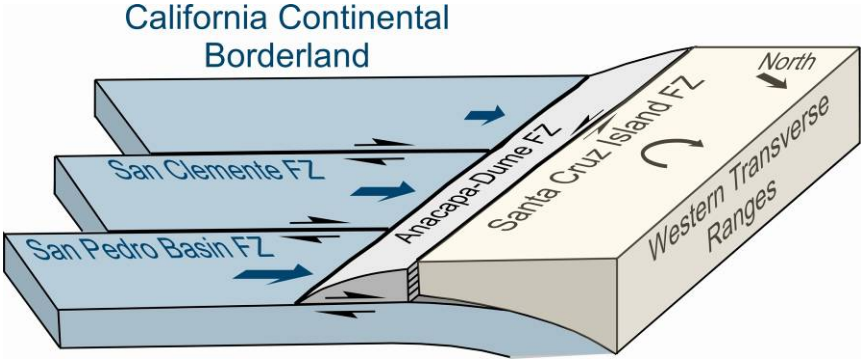

FIGURE 26. Model proposed for the Channel Islands. This type of scenario may be appropriate for the Santa Monica Mountains, modified from Legg and others, (2004).

The seismo-lineament method worked best in this case with a focal mechanism solution whose planes are almost vertical, so the uncertainty in the dip angle was minimized. Nodal planes that had high dip angles also have a smaller error region which makes field work even more efficient because of the smaller area that must be covered to look for the faults.

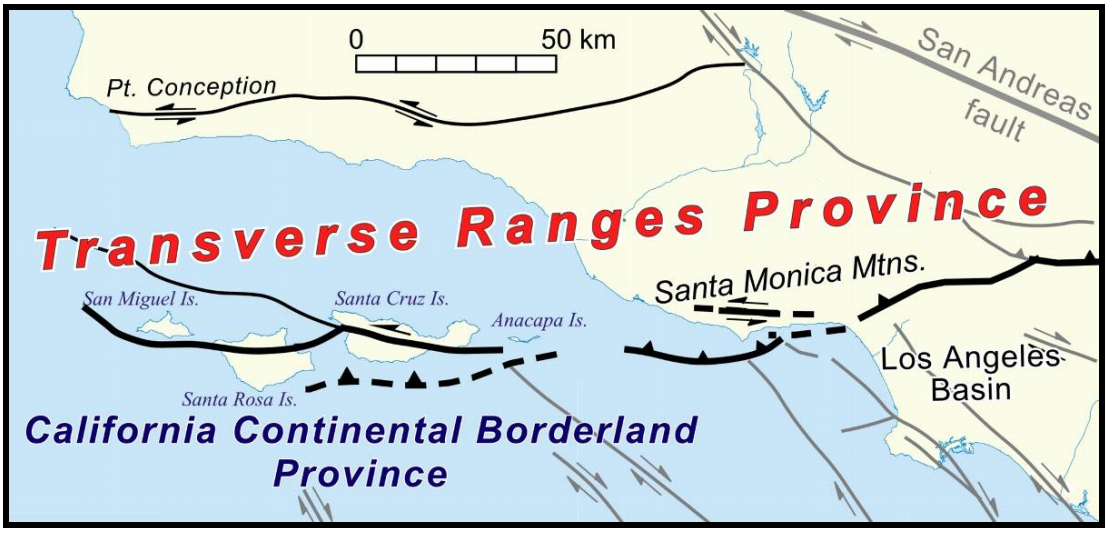

FIGURE 27. Regional map of the western transverse ranges showing the Channel Islands have a similar structural style the Santa Monica Mountains.

It is important to note that the seismo-lineaments investigated in this study, and the previously-unmapped faults encountered in the field, do not coincide with the Malibu Coast Fault Zone. This indicates that the Malibu Coast Fault Zone is not the only active fault structure in the Santa Monica Mountains. It is also interesting to note that the newly mapped faults traverse highland areas where they cut pre-Holocene formations exposed at the ground surface. An active fault in an eroding upland area may cut only pre-Holocene material at the surface, illustrating the limits associated with the practice of defining active faults only on the basis of trench studies or observed surface rupture during earthquakes.

This area has a high landslide hazard due to several factors: the weak rock, brief periods of heavy rainfall, seismicity of the area causing instability and many existing faults which can act as glide surfaces for slides and slumps. Landslides may make identifying faults more difficult by covering them; however landslides, can also help in the identification of active fault if they are offset and because they are geologically young they can assist in determining a faults activity.

Availability of finer resolution DEMs would improve the geomorphic lineament analysis by allowing the interpreter to see faults of smaller size. Other remote sensing data can also be utilized but were not within the scope of this particular study. The use of Landsat data would allow for vegetation indexes to be used as another tool for identifying lineaments and faults.

Conclusions

Several previously unidentified potentially active faults have been identified in the Point Dume 7.5 minute quadrangle. This test indicates that the projection of nodal planes from focal mechanism solutions onto a digital elevation map provides the basis for hypotheses which are testable in the field and are useful in identifying previously unmapped faults.

Active seismogenic faulting in the central Santa Monica Mountains does not appear to be confined to the strip immediately adjacent to the coastline and offshore areas, as is commonly assumed.

The newly discovered faults require additional study to identify locations where a trench might be established to resolve whether the fault cuts Holocene materials. Studies now underway will include additional earthquakes and a broader region of the central Santa Monica Mountains.

Improved understanding of the processes responsible for the active development of the Santa Monica Mountains and surrounding basins will aid future study in areas with similar structural history and style. This method is applicable to any area where Holocene material may not be available for trenching and where the instrumentation to obtain earthquake focal mechanism solutions exists.

APPENDICES

APPENDIX A

Example *Mathematica* Projection Code

```
startTime = AbsoluteTime[];
```

Projecting a fault plane from a focal mechanism solution onto a digital elevation model surface

Written and revised by Vince Cronin for a research project of Vince Cronin, Bruce Byars and Lisa Zygo

Begun August 5, 2004; Revised September 16, 2004

Introduction

The purpose of this notebook is to describe how to define the intersection of a DEM surface and a plane of given orientation that passes through a particular point located below the DEM surface. The application of this is in estimating the surface trace of a fault plane defined by an earthquake focal mechanism solution. It is hoped that this technique, in conjunction with structural terrain analysis and field mapping, will assist in the identification of the surface traces of active faults.

Description of input data

▪ From focal mechanism solution

Epicenter location: latitude (focalLat) and longitude (focalLong) in decimal degrees.

```
focalLat = 34.056;
```

```
focalLong = -118.821;
```

Focal depth (focalDepthKm) in kilometers

```
focalDepthKm = 11.18;
```

The central meridian of UTM Zone 11 is longitude -117°.

```
zoneMeridian = -117;
```

Trend (faultDipTrend) and plunge (faultDipPlunge) of dip vector of the fault plane, in decimal degrees

```
faultDipTrend = 185;
```

```
faultDipPlunge = 75;
```

▪ From the digital elevation model

The digital elevation model is presented as a set of z data in meters, with x and y coordinates explicit from the position of the z datum in the data file. The data file is derived from the U.S. Geological Survey's DEM data for the Pt. Dume, Malibu Beach and Topanga 7.5 minute quadrangles (30 m resolution), resampled to 10 m grid spacing. The header information includes the following:

"ncols" is the number of columns; label in position [[1,1]] and value in [[1,2]]

"nrows" is the number of rows; label in position [[2,1]] and value in [[2,2]]

"xllcorner" is the UTM zone 11 "x" coordinate of the lower left corner of the DEM; label in position [[3,1]] and value in [[3,2]].

"yllcorner" is the UTM zone 11 "y" coordinate of the lower left corner of the DEM; label in position [[4,1]] and value in [[4,2]]

"cellsize" is the distance between grid nodes in the DEM file, in meters; label in position [[5,1]] and value in [[5,2]]
Note that the code below uses the variable name "gridSpacing" rather than "cellsize."

"nodata_value" is the value used in the data file to indicate that there is no data in a specific location in the data file; label in position [[6,1]] and value in [[6,2]]

The seventh row of the data set is the first data row.

The true UTM coordinates of the datum in position [[i,j]] of the data set (from row 7 to the end) are as follows:

x coordinate = xllcorner + (cellsize * (j - 1)) y coordinate = yllcorner + (cellsize * (nrows - i))
z coordinate = the datum in position [[i,j]]

▪ Establish the width of the trace of the fault plane across the DEM

This is a user-defined factor that controls the approximate surface width of the computed trace of the fault plane across the DEM. The horizontal grid spacing is multiplied by this factor to specify the width of the trace of the fault plane on the DEM; for example, if the input factor is "2.5", the width of the fault trace will be approximately 2.5 times the grid spacing in the DEM. The larger the factor, the wider the fault trace.

```
traceWidthFactor = 2.5;
```

Description of algorithm

Each fault surface is initially represented by an upward-directed unit vector that is normal to the fault plane and whose origin is at the earthquake focus. Each location vector to a point on the DEM surface grid is evaluated to determine whether it is within a user-defined region around 90° from the vector normal to the fault. If so, that grid location is identified as being along the surface trace of the fault plane. The result of evaluating every point on the DEM surface grid in this manner will be a subset of points that collectively define the surface trace of the fault plane across the DEM surface.

▪ Some user-defined functions and conversion constants

```
makeVector[plunge_, trend_] := {Cos[plunge Degree] Sin[trend Degree],
   Cos[plunge Degree] Cos[trend Degree], -Sin[plunge Degree]};

vectorNorm[x_] := √(x.x);

unitVector[x_] :=
  {x[[1]] / vectorNorm[x], x[[2]] / vectorNorm[x], x[[3]] / vectorNorm[x]};

vectorAngle[a_, b_] := ArcCos[a.b / (vectorNorm[a] vectorNorm[b])];
```

The lat/long to UTM conversion is after Snyder, 1982.

```
convertToUTM[inLat_, inLong_, centMerid_] :=
  Module[{c1, c2, c3, c4, c5, v1, v2, v3, v4, v5, v6, utmX, utmY}, c1 = 6378206.4;
   c2 = 0.00676866; c3 = 0; c4 = centMerid; c5 = 0.9996; v1 = c2 / (1 - c2);
   v2 = c1 / Sqrt[1 - (c2 * (Sin[inLat Degree]^2))]; v3 = Tan[inLat Degree]^2;
   v4 = v1 * (Cos[inLat Degree]^2); v5 = (Cos[inLat Degree]) * ((inLong - c4) (π/180));
   v6 = (111132.0894 * inLat) - (16216.94 * Sin[2 * (inLat Degree)]) +
     (17.21 * Sin[4 * (inLat Degree)]) - (0.02 * Sin[6 * (inLat Degree)]);
   utmX = (c5 * v2 * (v5 + (((1 - v3 + v4) * v5^3) / 6) +
         ((5 - (18 * v3) + (v3^2) + (72 * v4) - (58 * v1)) * v5^5) / 120)) + 500000;
   utmY = c5 * (v6 - 0 + (v2 * Tan[inLat Degree] * ((v5^2 / 2) +
           (((5 - v3 + (9 * v4) + (4 * (v4^2))) * v5^4) / 24) + (((61 - (58 * v3) +
                 (v3^2) + (600 * v4) - (330 * v1)) * v5^6) / 720)))); {utmX, utmY}];
```

The following module differentiates between points that are within "width" meters from the fault plane and those that are further away. Given unit vector N that is normal to the fault plane that passes through the origin of the coordinate system, the distance from an arbitrary point (whose position vector is P) to that plane is given by |N·P|.

```
pointEvaluator[xCoord_, yCoord_, zCoord_, width_, fltUNrml_, nulData_] :=
  Module[{locVect, distToFlt, result}, locVect = {xCoord, yCoord, zCoord};
   distToFlt = If[(zCoord < (-1000)), 5 * width, Abs[Dot[fltUNrml, locVect]]];
   result = If[(distToFlt ≤ width), 1, nulData]; result];
```

▪ Find the unit vector normal to the fault surface at the earthquake focus

Convert the fault dip vector from trend and plunge to a unit location vector (dipUnitVector)

```
faultDipUnitVector = unitVector[makeVector[faultDipPlunge, faultDipTrend]];
```

Find the dip azimuth vector (dipAzimuthVector)

```
dipAzimuthVector = {Sin[faultDipTrend Degree], Cos[faultDipTrend Degree], 0};
```

Find the strike vector (strikeVector) defined using the right-hand rule

```
faultStrikeTrend = faultDipTrend - 90;

strikeVector = {Sin[faultStrikeTrend Degree], Cos[faultStrikeTrend Degree], 0};
```

Find the unit vector that is normal to the fault plane and is directed upwards (faultUnitNormal)

```
faultUnitNormal = unitVector[faultDipUnitVector × strikeVector];
```

■ Import and transform the DEM data

It is assumed that the DEM data is in a file called "xport.1" that is on the desktop, with the path "C:\\Documents and Settings\\Vince_Cronin\\Desktop\\xport1.dat"

```
mydata = Import[
   "C:\\Documents and Settings\\Brian_Bayliss\\Desktop\\rastert_malidem1.dat"];
```

Read the header information.

```
headerData = Table[mydata[[i, j]], {i, 6}, {j, 2}];

ncols = headerData[[1, 2]];

nrows = headerData[[2, 2]];

xllcorner = headerData[[3, 2]];

yllcorner = headerData[[4, 2]];

gridSpacing = headerData[[5, 2]];

nodataValue = headerData[[6, 2]];
```

■ Convert the input coordinates of the earthquake focus to the same coordinate system as the DEM data

```
utmCoordinates = convertToUTM[focalLat, focalLong, zoneMeridian];

focus = {(utmCoordinates[[1]] - xllcorner),
   (utmCoordinates[[2]] - yllcorner), (focalDepthKm * (-1000))};
```

■ Define the angular tolerance for resolving whether a point in the DEM is along the fault trace

Specify the approximate surface width of the trace of the fault plane across the DEM.

```
zoneHalfWidth = gridSpacing * traceWidthFactor / Sin[faultDipPlunge Degree];
```

■ Determine which points on the DEM lie along the modeled fault-plane trace, ± the traceWidth distance

The UTM coordinates of each point from the DEM are transformed to a coordinate system whose origin is at the earthquake focus (focus = {(utmCoordinates[[1]]-xllcorner),(utmCoordinates[[2]]-yllcorner),(focalDepthKm*(-1000))}).

x coordinate=(gridSpacing*(j-1))-focus[[1]] y coordinate=(gridSpacing*(nrows-1))-focus[[2]]
z coordinate=(the datum in position [[i,j]])-focus[[3]]

```
inFaultTrace = Table[pointEvaluator[((gridSpacing * (j - 1)) - focus[[1]]),
    ((gridSpacing * (nrows - i)) - focus[[2]]), (mydata[[i + 6, j]] - focus[[3]]),
    zoneHalfWidth, faultUnitNormal, nodataValue], {i, nrows}, {j, ncols}];

elev1 = Table[inFaultTrace[[i, j]], {i, nrows, 1, -1}, {j, ncols}];

traceImageFile =
 ListContourPlot[elev1, ContourShading → False, AspectRatio → Automatic]
```

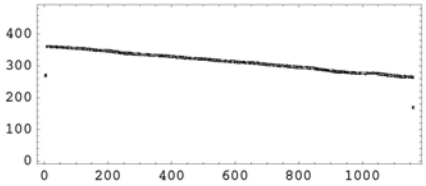


```
- ContourGraphics -

demImageFile = Table[mydata[[i + 6, j]] - focus[[3]], {i, nrows}, {j, ncols}];

aratio = nrows / ncols;
minval = 0;
maxval = Max[demImageFile];
relief = (maxval - minval);

elev2 = Table[demImageFile[[i, j]] + focus[[3]], {i, nrows, 1, -1}, {j, ncols}];

topoMap = ListContourPlot[elev2, ContourShading → False, Frame → False,
   AspectRatio → aratio, Contours → Table[c, {c, -200., 7000., 200.001}]];
```

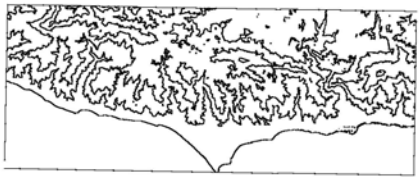

```
ListDensityPlot[elev2, AspectRatio → aratio, Frame → False,
  Mesh → False, ColorFunction → Function[z, GrayLevel[(0.3 + 0.7 z)]]];
```

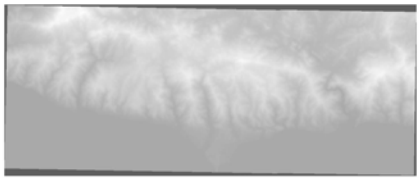

```
shadedTopoMap = Show[%, topoMap];
```

shadedTopoMap=ListContourPlot[elev2,AspectRatio→aratio,ColorFunction→Function[z,GrayLevel[(0.4+0.7z)]],-Contours→Table[c,{c,-125.,7000.,125.001}]]

```
finalImage = Show[shadedTopoMap, traceImageFile]
```

```
- Graphics -
```

■ Add the original header data to the output file

```
mergedData = Join[headerData, inFaultTrace];
```

■ Export the table of data along the fault trace ("pointsAlongFault.dat"), and a separate file containing only the header data ("header.dat")

```
Export["C:\\Documents and Settings\\Vince_Cronin\\Desktop\\
    BaylissMathematica\\Earthquake 1039\\traceFile1039a.dat", mergedData];
```

Export["C:\\Documents and Settings\\Vince_Cronin\\Desktop\\header.dat",headerData];

```
Export["C:\\Documents and Settings\\Vince_Cronin\\Desktop\\BaylissMathematica
    \\Earthquake 1039\\EQ1039aTraceOnly.eps", traceImageFile, "EPS"];

Export["C:\\Documents and Settings\\Vince_Cronin\\Desktop\\BaylissMathematica
    \\Earthquake 1039\\EQ1039aTraceMap.eps", finalImage, "EPS"];

Export["C:\\Documents and Settings\\Vince_Cronin\\Desktop\\BaylissMathematica
    \\Earthquake 1039\\EQ1039aMapOnly.eps", shadedTopoMap, "EPS"];
```

```
Export::nodir :
 Directory C:\Documents and Settings\Vince_Cronin\Desktop\BaylissMathematica\Earthquake 1039\\ does
   not exist. More…
```

```
ClearAll[mergedData, traceImageFile, finalImage,
  shadedTopoMap, mydata, inFaultTrace, elev1, elev2];
```

■ **How long did this program take to run, in minutes?**

```
minutesForProcessing = (AbsoluteTime[] - startTime) / 60
```

```
10.586636028
```

References

Colley, S.J., 2002, Vector calculus [2nd edition]: Upper Saddle River, New Jersey, Prentice-Hall, 558 p., (pp. 43-50), ISBN 0-13-041531-6.

Cronin, V.S., and Sverdrup, K.A., 1998, Preliminary assessment of the seismicity of the Malibu Coast Fault Zone, southern California, and related issues of philosophy and practice, *in* Welby, C.W., and Gowan, M.E. [editors], A Paradox of Power--Voices of Warning and Reason in the Geosciences: Geological Society of America, Reviews in Engineering Geology, p. 123-155.

Cronin, V.S., Byars, B.W., and Gammill, T., 2003, Developing techniques for regional structural interpretation using GIS and DEM-based terrain analysis: Geological Society of America, Abstracts with Programs, v. 34, no. 7, p. 261. http://gsa.confex.com/gsa/2003AM/finalprogram/abstract_61851.htm

Davis, H.F., and Snider, A.D., 1987, Introduction to vector analysis [5th edition]: Boston, Allyn and Bacon, 365 p. (pp. 34-37), ISBN 0-205-10263-8.

Gammill, T., Cronin, V.S., and Byars, B.W., 2004, Combining earthquake focal data and digital map analysis in reconnaissance for active faults, central Santa Monica Mountains and northern Santa Monica Bay, California: Geological Society of America, Abstracts with Programs,v. 36, no. 5, http://gsa.confex.com/gsa/2004-AM/finalprogram/abstract_80352.htm

Haneberg, W.C., 2004, Computational geosciences with *Mathematica*: Berlin, Springer-Verlag, 381 p., CD, ISBN 3-540-40245-4.

Snyder, J.P., 1982, Map projections used by the U.S. Geological Survey: U.S. Geological Survey Bulletin 1532, pp. 63-69 and 233-235.

APPENDIX B

Field Data and Fisher Statistics Data

Site A

	User-Supplied Input Values	
Number of measurements (N)	8	minimum = 3, maximum = 12
Instrument (compass) error	1.0	usually between 0.5° and 2°
Probability	0.10	0.05 for 95% CI
	Dip Azimuth/Trend (degrees)	Dip Angle/Plunge (degrees)
First measurement	345	80
Second measurement	20	80
Third measurement	0	80
Fourth measurement if any	355	80
Fifth measurement if any	10	82
Sixth measurement if any	15	81
Seventh measurement if any	15	79
Eighth measurement if any	8	75
Ninth measurement if any		
Tenth measurement if any		
Eleventh measurement if any		
Twelfth measurement if any		

	Output Values
Average dip azimuth/trend	6
95%CI uncertainty in strike/dip azimuth	11
Mean dip angle/plunge	80
Radius of 95% CI uncertainty cone	2
Estimate of k (class I if k≥10)	768

Site B

	User-Supplied Input Values	
Number of measurements (N)	8	minimum = 3, maximum = 12
Instrument (compass) error	1.0	usually between 0.5° and 2°
Probability	0.10	0.05 for 95% CI
	Dip Azimuth/Trend (degrees)	Dip Angle/Plunge (degrees)
First measurement	30	51
Second measurement	15	80
Third measurement	26	82
Fourth measurement if any	19	90
Fifth measurement if any	31	60
Sixth measurement if any	25	65
Seventh measurement if any	40	80
Eighth measurement if any	27	73
Ninth measurement if any		
Tenth measurement if any		
Eleventh measurement if any		
Twelfth measurement if any		

	Output Values
Average dip azimuth/trend	28
95%CI uncertainty in strike/dip azimuth	27
Mean dip angle/plunge	73
Radius of 95% CI uncertainty cone	8
Estimate of k (class I if k≥10)	38

Site C

User-Supplied Input Values		
Number of measurements (N)	9	minimum = 3, maximum = 12
Instrument (compass) error	1.0	usually between 0.5° and 2°
Probability	0.10	0.05 for 95% CI
	Dip Azimuth/Trend (degrees)	Dip Angle/Plunge (degrees)
First measurement	8	80
Second measurement	20	85
Third measurement	15	80
Fourth measurement if any	340	67
Fifth measurement if any	335	70
Sixth measurement if any	27	78
Seventh measurement if any	10	75
Eighth measurement if any	357	69
Ninth measurement if any	8	75
Tenth measurement if any		
Eleventh measurement if any		
Twelfth measurement if any		

	Output Values
Average dip azimuth/trend	359
95%CI uncertainty in strike/dip azimuth	18
Mean dip angle/plunge	76
Radius of 95% CI uncertainty cone	4
Estimate of k (class I if k≥10)	119

Site D

User-Supplied Input Values		
Number of measurements (N)	12	minimum = 3, maximum = 12
Instrument (compass) error	1.0	usually between 0.5° and 2°
Probability	0.10	0.05 for 95% CI
	Dip Azimuth/Trend (degrees)	Dip Angle/Plunge (degrees)
First measurement	335	85
Second measurement	337	65
Third measurement	305	80
Fourth measurement if any	162	83
Fifth measurement if any	145	90
Sixth measurement if any	315	82
Seventh measurement if any	334	80
Eighth measurement if any	335	82
Ninth measurement if any	157	85
Tenth measurement if any		
Eleventh measurement if any		
Twelfth measurement if any		

	Output Values
Average dip azimuth/trend	326
95%CI uncertainty in strike/dip azimuth	indeterminate
Mean dip angle/plunge	84
Radius of 95% CI uncertainty cone	23
Estimate of k (class I if k≥10)	4

Site E

User-Supplied Input Values		
Number of measurements (N)	12	minimum = 3, maximum = 12
Instrument (compass) error	1.0	usually between 0.5° and 2°
Probability	0.10	0.05 for 95% CI
	Dip Azimuth/Trend (degrees)	Dip Angle/Plunge (degrees)
First measurement	85	82
Second measurement	81	79
Third measurement	66	81
Fourth measurement if any	59	72
Fifth measurement if any	60	74
Sixth measurement if any	70	80
Seventh measurement if any	85	70
Eighth measurement if any	59	73
Ninth measurement if any	50	72
Tenth measurement if any	65	61
Eleventh measurement if any	52	88
Twelfth measurement if any	20	86

	Output Values
Average dip azimuth/trend	65
95%CI uncertainty in strike/dip azimuth	18
Mean dip angle/plunge	77
Radius of 95% CI uncertainty cone	4
Estimate of k (class I if k≥10)	97

REFERENCES

Bayliss, B., and Cronin, V.S., 2005, Test of a method for recognizing previously unmapped seismogenic faults: Geological Society of America, Abstracts with Programs, v. 37, no. 7, p. 559. http://gsa.confex.com/gsa/2005AM/finalprogram/abstract_94440.htm

Beck, M.E., Jr., 1983, On the mechanism of tectonic transport in zones of oblique subduction: Tectonophysics, v. 93, p. 1-11.

——— 1984, Has the Washington-Oregon Coast Range moved northward? Geology, v. 12, p. 737-740.

Biddle, K.T., [editor], 1991, Active margin basins: American Association of Petroleum Geologists, Memoir 52, p. 35-134.

Blake, G.H., 1991, Review of Neogene biostratigraphy and stratigraphy of the Los Angeles Basin and implications for basin evolution, *in* Biddle, K.T., [editor], Active margin basins: American Association of Petroleum Geologists, Memoir 52, p. 135-184.

Buika, J.A., and Teng, T.L., 1979, A seismicity study for portions of the Los Angeles basin, Santa Monica basin, and Santa Monica mountains, California: University of Southern California, Geophysical Laboratory, Technical Report 79-9, 191 p.

Burbank, D.W., and Anderson, R.S., 2001, Tectonic geomorphology: Oxford, Blackwell Science, 274 p.

Campbell, R.H., Blackerby, B.A., Yerkes, R.F., Schoellhamer, J.E., Birkeland, P.W., and Wentworth, C.M., 1996, Geologic map of the Point Dume quadrangle, Los Angeles County, California: U.S. Geological Survey Geologic Quadrangle Map GQ-4747. http://ngmdb.usgs.gov/ImageLibrary/ILview_xsl.html?sid=q24_61691_us_c.sid

Chester, F.M., Chester, J.S., Kirschner, D.L., Schulz, S.E., and Evans, J.P., 2004, Structure of large-displacement, strike-slip fault zones in the brittle continental crust, *in* Karner, G.D., Taylor, B., Driscoll, N.W., and Kohlstedt, D.L., [editors], Rheology and deformation of the lithosphere at continental margins: New York, Columbia University Press, p. 223-260.

Cronin, V.S., 2004, Projecting a fault plane from a focal mechanism solution onto a digital elevation model surface: unpublished *Mathematica* code.

——— 2006, Lineament analysis: unpublished draft manuscript.

——— 2007, Finding the mean and 95% confidence interval of a set of strike-and-dip or lineation data: Environmental and Engineering Geoscience*, in press*.

Cronin, V.S., and Sverdrup, K.A., 1998, Preliminary assessment of the seismicity of the Malibu Coast Fault Zone, southern California, and related issues of philosophy and practice, *in* Welby, C.W., and Gowan, M.E. [editors], A paradox of power--Voices of warning and reason in the geosciences: Geological Society of America, Reviews in Engineering Geology, p. 123-155.

Cronin, V.S., Byars, B.W., and Gammill, T., 2003, Developing techniques for regional structural interpretation using GIS and DEM-based terrain analysis: Geological Society of America, Abstracts with Programs, v. 34, no. 7, p. 261.

Cronin, V.S., Schurter, G.J., and Sverdrup, K.A., 1993, Preliminary Landsat lineament analysis of the northern Nanga Parbat-Haramosh Massif, northwest Himalaya, *in* Treloar, P.J., and Searle, M.P., [editors], Himalayan tectonics: Geological Society (London), Special Publication, No. 74, p. 193-206.

Davis, T. L., Namson, J.S., and Yerkes, R.F., 1989, A cross section of the Los Angeles area: seismically active fold and thrust belt, the 1987 Whittier Narrows earthquake, and earthquake hazard: Journal of Geophysical Research, v. 94, p. 9644–9664.

Dibblee, T.W., Jr., and Ehrenspeck, H.E., 1993, Geologic map of the Point Dume Quadrangle, Los Angeles County, California: Dibblee Geological Foundation Map DF-48, scale 1:24,000.

Dolan, J. F., Sieh , K., Rockwell, T.K., Yeats, R.S., Shaw, J., Suppe, J., Huftile, G., and Gath, E., 1995, Prospects for larger or more frequent earthquakes in greater metropolitan Los Angeles, California: Science, v. 267, p. 199–205.

Dolan, J. F., Sieh, K., and Rockwell, T.K., 2000, Late Quaternary activity and seismic potential of the Santa Monica fault system, Los Angeles, California: Geological Society of America Bulletin, v.112, p.1559–1581

Drumm, P.L., 1992, Holocene displacement of the central splay of the Malibu Coast fault zone, Latigo Canyon, Malibu, *in* Pipkin. B.W., and Proctor, R.J., [editors], Engineering geology practice in southern California: Belmont, California, Star Publishing Company, Association of Engineering Geologists, Southern California Section, Special Publication No. 4, 247-254.

Fisher, M.A., Langenheim, V.E., Sorlien, C.C., Dartnell, P., Sliter, R.W., Cochrane, G.R., and Wong F.L, 2005, Recent deformation along the offshore Malibu Coast, Dume, and related faults west of Point Dume, southern California: Bulletin of the Seismological Society of America, v. 95, no. 6, p. 2486–2500

Fuis, G.S., and 14 others, 2003, Fault systems of the 1971 San Fernando and 1994 Northridge earthquakes, southern California - relocated aftershocks and seismic images from LARSE II: Geology, v. 31, no. 2, p.171-174.

Gammill, T., Cronin, V.S., and Byars, B.W., 2004, Combining earthquake focal data and digital map analysis in reconnaissance for active faults, central Santa Monica Mountains and northern Santa Monica Bay, California: Geological Society of America, Abstracts with Programs, v. 36, no. 5, p. 298.

Haneberg, W.C., 2004, Computational geosciences with *Mathematica*: Berlin, Springer-Verlag, 381 p., CD.

Hardebeck, J.L., 2005, SCEDC web dataset: Southern California Earthquake Data Center, http://www.data.scec.org/research/socal_focal_JLH.html.

Hardebeck, J.L., and Shearer, P.M., 2003, Using S/P amplitude ratios to constrain the focal mechanisms of small earthquakes: Bulletin of the Seismological Society of America, v. 93, p. 2434-2444.

Hart, E.W., and Bryant, W.A., 1999, Fault-rupture hazard zones in California: Special Publication 42, California Department of Conservation Division of Mines and Geology, ftp://ftp.consrv.ca.gov/pub/dmg/pubs/sp/Sp42.pdf

Haugerud, R.A., Harding, D.J., Johnson, S.Y., Harless, J.L., Weaver, C.S., and Sherrod, B.L., 2003, High-resolution LIDAR topography of the Puget lowland, Washington – a bonanza for Earth science: GSA Today, v. 13, no. 6, p. 4-10, ftp://rock.geosociety.org/pubs/GSAToday/gt0306.pdf

Hauksson, E., 1987, Seismotectonics of the Newport-Inglewood fault zone in the Los Angeles Basin, southern California: Bulletin of the Seismological Society of America, v. 77, p. 539–561.

——— 1990, Earthquakes, faulting, and stress in the Los Angeles Basin: Journal of Geophysical Research, v. 95, p. 15,365-15,394.

——— 2000, Crustal structure and seismicity distribution adjacent to the Pacific and North America plate boundary in southern California: Journal of Geophysical Research, v. 105, p. 13,875-13,903.

——— 2004, 3-D earthquake focal mechanisms: Southern California Earthquake Data Center, http://www.data.scec.org/research/socal_focal.html

Hauksson, E., and Saldivar, G V, 1986, The 1930 Santa Monica and the 1979 Malibu, California, earthquakes: Bulletin of the Seismological Society of America, v. 76, p. 1542-1559.

Hauksson, E., and Saldivar, G.V., 1989, Seismicity and active compressional tectonics in Santa Monica Bay, southern California: Journal of Geophysical Research, v. 94, no. B7, p.9591-9606.

Hill, R.L., 1979, Potrero Canyon fault and University High School escarpment, *in* Keaton, J., editor, Field guide to selected engineering geologic features, Santa Monica Mountains: Los Angeles, California, Association of Engineering Geologists, Southern California Section, Field Trip Guidebook, p. 83-103.

Hobbs, W.H., 1904, Lineaments of the Atlantic border region: Geological Society of America Bulletin, v. 15, p. 483-506.

Hoots, H.W., 1931, Geology of the eastern part of the Santa Monica Mountains, Los Angeles County, California: U.S. Geological Survey, Professional Paper 165-C, p. 83-134, map scale 1:24,000.

Hornafius, J.S., Luyendyk, B.P., Terres, R.R., and Kamerling, M.J., 1986, Timing and extent of Neogene tectonic rotation in the western Transverse Ranges, California: Geological Society of America Bulletin, v. 97, p. 1476-1487

Kamerling, M.J., and Luyendyk, B.P., 1979, A model for Neogene tectonics of the inner southern California borderland constrained by paleomagnetic data: Geological Society of America, Abstracts with Programs, v. 11, no. 7, p. 453.

——— 1985, Paleomagnetism and Neogene tectonics of the northern Channel Islands, California: Journal of Geophysical Research, v. 90, p. 12485–12,502.

Keller, E.A., and Pinter, N., 2002, Active tectonics -- earthquakes, uplift and landscape [second edition]: Upper Saddle River, New Jersey, Prentice Hall, 362 p.

Lajoie, K.R., Kern, J.P., Wehmiller, J.F., Kennedy, G.L., Mathieson, S.A., Sarna-Wojcicki, A.M., Yerkes, R.F., and McCrory, P.F., 1979, Quaternary marine shorelines and crustal deformation, San Diego to Santa Barbara, California, *in* Abbott, P.L., [editor], Geological excursions in the southern California area: Department of Geological Sciences, San Diego State University, for Geological Society of America Annual Meeting, Nov. 1979, p. 3-15.

Larson, K.M., 1993, Application of the global positioning system to crustal deformation measurements 3, Results from the southern California borderlands: Journal of Geophysical Research, v. 98, p. 21713–21726.

Lee, W.H.K., Yerkes, R.F., and Simirenko, M., 1979, Recent earthquake activity and focal mechanisms in the western Transverse Ranges, California: U.S. Geological Survey Circular 799-A, 26 p.

Legg, M.R., Kamerling, M.J., and Francis, R.D., 2004, Termination of strike-slip faults at convergence zones within continental transform boundaries -- examples from the California Continental Borderland, *in* Grocott, J., McCaffrey, K.J.W., Taylor, G., and Tikoff, B., [editors], Vertical coupling and decoupling in the lithosphere: Geological Society, London, Special Publication 227, p. 65-82.

Lillesand, T.M., and Kiefer, R.W., 1987, Remote sensing and image interpretation [2nd edition]: New York, John Wiley & Co., 721 p.

Lobeck, A.K., 1939, Geomorphology – an introduction to the study of landscapes: New York, McGraw-Hill Book Company, 731 p.

Luyendyk, B.P., 1991, A model for Neogene crustal rotations, transtension and transpression in California: Geological Society of America Bulletin, v.103, p. 1528-1536.

Luyendyk, B.P., Kamerling, M.J, and Terres, R.R., Hornafius, S.J., 1985, Simple shear of southern California during Neogene time suggested by paleomagnetic declinations: Journal of Geophysical Research, v. 90, p. 12454-12466.

Maune, D.F., 2001, Digital elevation model technologies and applications: The DEM user's manual: Bethesda, Maryland, American Society for Photogrammetry and Remote Sensing, 539 p.

McCalpin, J.P., [editor], 1996, Paleoseismology: San Diego, Academic Press, 588 p.

Miller, V.C., 1961, Photogeology: New York, McGraw-Hill Book Company, 248 p.

Molnar, P., and Gibson, J. M., 1994, Very long baseline interferometry and active rotations of crustal blocks in the western Transverse Ranges, California: Geological Society of America Bulletin, v. 106, p. 594–606

Nicholson, C., Sorlien, C.C., Atwater, T., Crowell, J.C., and Luyendyk, B.P., 1994, Microplate capture, rotation of the western Transverse Ranges, and initiation of the San Andreas transform as a low-angle fault system: Geology, v. 22, p. 491–495.

Petersen, M.D., and Wesnousky, S.G., 1994, Fault slip rates and earthquake histories for active faults in southern California: Bulletin of the Seismological Society of America, Vol. 84, No. 5, pp. 1608-1649,

Pinter, N., Lueddecke, S.B., Keller, E.A., and Simmons, K.R., 1998, Late Quaternary slip on the Santa Cruz Island fault, California: Geological Society of America Bulletin, v. 110, no. 6, p. 711–722.

Ray, R.G., 1960, Aerial photographs in geologic interpretation and mapping: U.S. Geological Survey, Professional Paper 373, 230 p.

Scholz, C.H., 2002, The mechanics of earthquakes and faulting [second edition]: Cambridge University Press, 471 p.

Seeber, L., and Sorlien, C.C., 2000, Listric thrusts in the western Transverse Ranges, California: Geological Society of America Bulletin, v. 112, no. 7, p. 1067–1079.

Snyder, J.P., 1982, Map projections used by the U.S. Geological Survey: U.S. Geological Survey, Bulletin 1532, 313 p.

Stierman, D.J., and Ellsworth, W.L., 1976, Aftershocks of the February 21, 1973, Point Mugu, California, earthquake: Bulletin of the Seismological Society of America, v. 66, p. 1931-1952.

Tsutsumi**,** H., Yeats, R.S., and Huftile, G.J., 2001, Late Cenozoic tectonics of the northern Los Angeles fault system, California: Geological Society of America Bulletin, v. 113, no. 4, p. 454–468.

Treiman, J.A., 1994, Malibu Coast fault, Los Angeles County, California: California Department of Conservation, Division of Mines and Geology, unpublished Fault Evaluation Report FER-229, October 3, 1994, 42 p.

——— [compiler], 2000, Fault number 99, Malibu Coast fault, *in* Quaternary fault and fold database of the United States, ver 1.0: U.S. Geological Survey Open-File Report 03-417.

U.S. Geological Survey, 1995, Point Dume, California 7.5 Minute Quadrangle: U.S. Geological Survey 7.5 Minute Series, 1 sheet, scale 1:24,000.

Webb, T.H., and Kanamori, H., 1985, Earthquake focal mechanisms in the eastern Transverse Ranges and San Emigdio Mountains, southern California and evidence for a regional decollement: Bulletin of the Seismological Society of America, v. 75, p. 737-757.

Wesnousky, S. G., 1986, Earthquakes, Quaternary faults, and seismic hazard in California: Journal of Geophysical Research, v. 91, p. 12587–12631.

Wesson, R.L., Helley, E.J., Lajoie, K.R., and Wentworth, C.M., 1975, Faults and future earthquakes, *in* Borcherdt, R.D., [editor], Studies for seismic zonation of the San Francisco Bay region: U.S. Geological Survey, Professional Paper 941-A, p. 5-30.

Worchester, P.G., 1948, A textbook of geomorphology: Toronto, D. Van Nostrand Company, 584 p.

Wright, T.L., 1991, Structural geology and tectonic evolution of the Los Angeles Basin, California, *in* Biddle, K.T., [editor], Active margin basins: American Association of Petroleum Geologists Memoir 52, p. 35-134.

Yerkes, R.F., and Campbell, R.H., 1980, Geologic map of east-central Santa Monica Mountains, Los Angeles County, California: U.S. Geological Survey, Map I-1146, scale 1:24,000.

Yerkes, R.F., and Wentworth, C.M., 1965, Structure, Quaternary history, and general geology of the Corral Canyon area, Los Angeles County, California: U.S. Geological Survey, Open-File Report 864, 214 p.

Ziony, J. K., and Yerkes, R. F., 1985, Evaluating earthquake and surface faulting potential, *in* Ziony. J. I., [editor], Evaluating earthquake hazards in the Los Angeles region—An Earth-science perspective: U.S. Geological Survey, Professional Paper 1360, p. 43-91.